Identification of Achondritic Meteorite Parentage by Handheld Energy Dispersive X-ray Fluorescence Spectrometry

Maurizio GEMELLI[1*], Tommaso DI ROCCO[1**], Luigi FOLCO[1], and Massimo D'ORAZIO[1]

[1]Dipartimento di Scienze della Terra, Università di Pisa, via S. Maria 53, 56126 Pisa, Italy

*Corresponding author. E-mail: maurizio.gemelli@unipi.it; tel. +390502215726

[**]Currently at Istituto di Geoscienze e Georisorse, CNR, Pisa, Via Moruzzi, 1 Pisa, Italy

Abstract – We evaluate the potential of a handheld energy dispersive XRF spectrometer for the preliminary classification of non-chondritic differentiated meteorites. The studied achondrites include: 9 lunar meteorites, 17 Martian meteorites, 5 angrites and 18 meteorites from asteroid 4 Vesta. Analytical precision and accuracy was tested on 39 terrestrial igneous rock slabs showing a wide range of composition.

Replicate analyses, performed on the studied meteorites show that Fe/Mn values together with Si and Ca/K ratio can be used in the discrimination of different achondrite groups. Fusion crust's Fe/Mn values of meteorites from Vesta and Mars are indistinguishable from those of the interior implying that even measurements on the external surface could be sufficient to pigeonhole non-chondritic meteorites. Handheld energy dispersive XRF spectrometer is a non-destructive but very effective technique for preliminary classification of achondrites in the field and in laboratory and reclassification of mislabelled meteorites in the museums.

Keywords: handheld XRF, meteorite, achondrite, planetary basalts

Introduction

Differentiated achondrites are a group of stony meteorites, comprising about 5% of all meteorites.

Differentiated achondrites are igneous rocks from asteroids and planetary bodies of great interest for planetary science. Their cosmochemical study provides unique insights into magmatic differentiation processes that have occurred on the largest rocky bodies of the Solar System since its very beginning about 4.56 Ga ago (Halliday and Kleine 2006 and reference therein). Several methods are used to discriminate differentiated achondrites and to establish their planetary parentage. Among them, triple oxygen isotopes technique is probably the most powerful to identify their parent bodies and genetic relationships between meteorites. This is mainly because oxygen displays a large (per mil) mass-independent fractionation among solar system bodies (e.g., Clayton and Mayeda 1996).

Major-, minor- and trace-elements concentrations and element ratios in bulk rock and silicate minerals (e.g., olivine, pyroxene and plagioclase) are also largely used to establish the specific planetary body source (Cameron and Papike 1981, Goodrich and Delaney 2000, Mittlefehldt 2014) as compositional differences may reflect the different physical-chemical conditions (e.g., T, P, fO_2) and processes (e.g., planetary differentiation, fractional melting and crystallization, and differentiation through impact) that occur on the various planetary or asteroidal bodies.

These techniques require, however, considerable sample preparation, are expensive and destructive. Among the few non-destructive analytical techniques, magnetic susceptibility, in combination with porosity and density data, and handheld energy dispersive X-ray fluorescence (HH-EDXRF) are the most common (Rochette *et al.* 2003, Gattacceca *et al.* 2004, Macke *et al.* 2011, Zurfluh *et al.* 2011, Gemelli *et al.* 2015, Young *et al.* 2016) . Although very powerful for fresh (or nearly so) meteorites, magnetic susceptibility may give problematic classification results whenever terrestrial weathering changes the original magnetic signal (Kohout *et al.* 2004, Macke *et al.* 2011, Rochette and Gattacceca 2012).

HH-EDXRF is rapidly gaining recognition for numerous applications. These applications include the determination of metals in soils (Kalnicky and Singhvi 2001, Radu and Diamond 2009, Wu *et al.* 2012,) and sediments (Kirtay *et al.* 1998, Kenna *et al.* 2011), analysis of artefacts and artworks

(Liritzis and Zacharias 2011, Vázquez *et al.* 2012, Comelli *et al.* 2016), quality tests in the metallurgical industry and engineering, and the identification and classification of hazardous wastes (Vanhoof *et al.* 2013). Recently, HH-EDXRF has been used to identify and classify different groups of stony meteorites (Zurfluh *et al.* 2011), to perform chemical bulk analysis on iron meteorites (Gemelli *et al.* 2015) and to evaluate its potential in planetary surface exploration (Young *et al.* 2016). The reasons for the significant success of HH-EDXRF (Potts and West 2009) include: i) portability of the instrument, ii) easy handling of the operating system, iii) minimal sample preparation iv) rapid, non-destructive analyses with remarkable reproducibility and relative low detection limits for elements heavier than Na.

Among differentiated achondrites, the Howardite, Eucrite, Diogenite (HED) group, is believed to be genetically linked to the asteroid 4 Vesta (e.g., McCord *et al.* 1970, Consolmagno and Drake 1977). Excluding Earth and Moon, HED constitutes the largest group of crustal igneous rocks available from a single body of the solar system (Mittlefehldt *et al.* 1998).

Shergottites, Nakhlites and Chassignites (SNC) and orthopyroxenite ALH 84001 are basalts and ultramafic rocks from a single parent body on the basis of their similar $\Delta^{17}O$ values (~ 0.32; Clayton and Mayeda 1996, Franchi *et al.* 1999, Wiechert *et al.* 2001). The young crystallization ages and the occurrence of gas entrapped in fluid inclusions in the constituent minerals with composition similar to the Martian atmosphere, were the first strong evidence supporting the hypothesis that the SNC meteorites come from Mars (McSween 1994, Treiman *et al.* 2000). More recently data collected by orbital and landed spacecraft missions (e.g., McCoy *et al.* 2011) proved that SNCs are actually samples of the surface of Mars.

The Apollo and Luna missions returned over 380 kg of samples from a limited portion of the Moon's nearside. Lunar meteorites are substantially identical to the returned samples and represent a random sampling of the entire lunar surface. Therefore, they can provide invaluable insights into the unsampled terrains of the Moon and are fundamental for determining the composition of the bulk lunar crust (e.g., Jolliff *et al.* 2000, Korotev *et al.* 2003, Demidova *et al.* 2007, Korotev *et al.*

2009,Taylor 2009, Joy *et al.* 2010, Kobayashi *et al.* 2010, Yamaguchi *et al.* 2010)

Angrites are a small, rare and unusual grouplet of mafic volcanic and plutonic rocks consisting of eleven meteorites (Keil 2012). On the basis of petrographic observations and the low volatile elements content it has been suggested that they might derive from Mercury (e.g., Papike *et al.* 2003, Irving *et al.* 2005, Irving *et al.* 2006, Kuehner *et al.* 2006, Kuehner and Irving 2007). Their high FeO contents, however, is in contradiction with the low FeO content of Mercury's surface rocks indicated by spectral properties. On the basis of spectral reflectance data, Burbine *et al.* (2001, 2006) suggest a possible kinship between angrites and the asteroids 289 Nenetta and 3819 Robinson. The importance of angrites, however, mainly resides in the fact that they are approximately only 4 Ma younger than calcium-aluminum-rich inclusions CAIs (e.g., Bouvier and Wadhwa 2010; Keil 2012) and record some of the earliest volcanic activity in the solar system.

The aim of this study is to provide an analytical protocol for an accurate determination of key elements by HH-EDXRF, such as Mg, Al, Si, P, K, Ca, Ti, Mn and Fe, useful for classification of meteorites. Here we present HH-EDXRF measurements of 49 differentiated achondrites consisting of 18 HEDs, 17 SNCs, 9 lunar meteorites and 5 angrites. Our data show that the combined use of different interelement ratios obtained by HH-EDXRF analyses such as Fe/Mn, Si and Ca/K and can be used for the discrimination of these four major groups of achondrites. This has important bearing for curatorial purposes, particularly when dealing with large collections of meteorites.

Analytical methods and materials

Instrument details

The instrument used in this study is a NITON XL3t GOLDD+ XRF spectrometer. It is equipped with a miniaturized X-ray tube (max 4W) with an Ag anode and a silicon drift detector (SDD) capable of acquiring spectra at high-count rates. The experimental routine used for this work

consists in three excitation steps with an overall measurement time of 150 s: 'main' (excitation 50 kV, 40 μA, Al-Fe filter, 50 s), 'low' (15 kV, 133 μA, Fe filter, 50 s) and 'light' (8 kV, 200 μA, no filter, 50 s). The list reporting measured elements and operative conditions is shown in Table 1. The instrument is designed for field use but it can also be mounted on a test stand with a shielded box protecting the user from radiation. During all analyses, the HH-EDXRF device was fixed in a mobile test stand in order to provide reproducible measurement conditions (Figure 1). Samples were positioned accurately in the analytical plane of the HH-EDXRF instrument and no additional corrections for air gap were required. The used beam diameter was 8 mm (Figure 2). Data reduction was carried out through the on-board software of the instrument using a 'Fundamental Parameters' correction algorithm. The obtained data were transferred on a computer using the Niton Data Transfer 8.0.1 software, by Thermo Scientific, Waltham, Massachusetts, USA.

Terrestrial samples

A set of thirty-nine terrestrial igneous rocks has been used for instrument calibration (Table S1 in Supporting Information).

A minimal sample preparation was carried out. It consisted of cutting of the samples in thick slabs by means of a diamond blade and grinding of the surface to minimize roughness using silicon carbide sandpapers (down to 400 mesh). Since rocks can be internally heterogeneous, 5 measurements for each slab were conducted and the average was taken.

The bulk composition of the same rocks was determined by wavelength dispersive XRF (WD-XRF), as well (Table S1). Samples for WD-XRF were powdered and ignited at 1000 °C for 1 hour. About 1 g of each ignited sample was fluxed with an excess of $Li_2B_4O_7$ (in a 1:7 ratio) to obtain a series of glass beads, which were analysed using a Thermo Fisher ARL 9400 XP spectrometer calibrated against 22 international reference rock standards (see Tamponi *et al.* 2003 for further details).

Meteorite samples

The meteorites selected for HH-EDXRF analysis include angrites, basaltic and ultramafic rocks from Moon, Mars and Vesta. Differentiated achondrites represent the products of igneous processes (i.e. partial to complete melting of the source rock, and magmatic crystallization) acting on asteroidal and planetary bodies (Mittlefehldt 2014). Therefore, differentiated achondrites match nicely the matrix of terrestrial igneous rocks used for calibration. Specimens are from National History Museum of London (NHM), Museo del Cielo e della Terra of San Giovanni in Persiceto (MCT), Museo Nazionale dell'Antartide of Siena (MNA), and the private collection of one of us (MDO) (Table 2). Given the large beam diameter (8 mm), the selected meteorites were chosen without any specific textural and granulometric constraints (Figure 2). However, attention was given to nominally heterogeneous samples (e.g. regolithic breccias, HED breccias, coarse-grained ultramafic rocks). Accordingly, different specimens of the same meteorites (i.e. Millbillillie, Camel Donga, Nakhla, SaU 008, Chassigny and D'Orbigny), available in at least two collections (i.e. NHM, MCT, MNA), were measured. Most of the meteorite samples used in this work consists of slabs and slices, of at least ~2 mm in thickness, with few fragments and fusion crusted fragments. The majority of analysed meteorites had at least one smooth-flat surface and when such surfaces were not available, the flattest, most even surface was analysed. When possible, the fusion crusted fragments were also analysed on the external surface.

Measurements were performed without any specific sample pre-treatment or preparation. Five spot analyses, in a few cases partially overlapping with each other (e.g. Figure 2b), were performed on 36 meteorites (measured area per sample ≤ 2.5 cm^2). Three spot analyses were run on the remaining thirteen samples due to their relatively smaller size (measured area per sample = 1.5 cm^2). They include four lunar meteorites (Dag 400, Dag 262, Dhofar 908, NWA 773), four SNCs (Nakhla, NWA 7397, SaU 008, Zagami), two HEDs (Dhofar 018, Johnstown) and three angrites (D'Orbigny,

NWA2999, Sahara 99555), (Table 2). The average of each measurement run was taken.

Results

Raw HH-EDXRF data for igneous terrestrial rock slabs are plotted in Figure 3 versus WD-XRF data. In each plot the regression lines (y=mx+q), the coefficient of determination (R^2) and the line of equality are reported. The equations of the regression lines are used to apply correction factors and improve the accuracy of the data for the element of interest. For most elements, the R^2 of the regression is very high. In particular, a very good correlation (i.e. $R^2 > 0.9$) is obtained for elements such as Si, K, Ca, Ti, Mn and Fe. For Mg, P and Al, lower R^2 of 0.89, 0.75 and 0.24 are obtained, respectively. This is not unexpected since Mg and Al are the lightest measurable elements by HH-EDXRF and P is generally in very low concentration. The precision, expressed as 1 SD, is < ±0.30 for Fe, Ca, Al and Mg, ~±0.5 for Si and <±0.07 for K, P, Ti and Mn.

Limit of Detection (LOD), calculated as three times the standard deviation of the concentration measured in samples with none or only a trace amount of the analyte, are 0.44 % m/m for Mg, 0.03 % m/m for P and 0.003 % m/m for Ti. Limits of detection for the other elements are not reported here since their concentrations are orders of magnitude above LOD in the studied samples.

Corrected HH-EDXRF values of igneous terrestrial rock slabs are reported in Table S1 and plotted in Figure 4. Figure 4 shows that the applied calibration is very efficient as demonstrated by the closeness of the data points to the 1:1 line plotted for reference. The accuracy of measurements is on average better than 7% for elements like Al, Si, K, Ca, Ti, Mn and Fe, ~12% for Mg and ~16% for P.

The corrected compositions of 49 meteorites is reported in Table 3. Raw data were corrected using equations obtained in Figure 3.

Discussion

Fe/Mn ratio

During field research, collection and initial characterization misclassifications of meteorites can occur (e.g., Lindstrom *et al.* 1994). For example, unaltered lunar and HEDs as well as Martian orthopyroxenite and diogenites can be similar at first sight and are hard to distinguish simply on the basis of their petrographic features. On the other hand, lunar meteorites and angrites as well as HEDs and SNCs although macroscopically distinct can shows similarities in their mineral and bulk chemistry (Fig 6; Papike 1998).

One of the most powerful tool to identify specific planetary body source (i.e. Earth, Mars, Moon, 4 Vesta, and angrite parent body) is the Fe/Mn ratio. This ratio can be used as a marker for the oxidation state of parent bodies as Fe and Mn show similarities in both valence state and ionic radii and do not fractionate during igneous processes. Wänke *et al.* (1973) first discovered the differences in the Fe/Mn ratio between bulk mesosiderites and HEDs. Papike *et al.* (2003) have found that Fe/Mn atomic ratio in olivine and pyroxene varies between planetary and asteroidal meteorites (i.e. $Fe/Mn_{angrites} > Fe/Mn_{lunar} > Fe/Mn_{Earth} > Fe/Mn_{SNCs} > Fe/Mn_{HEDs}$) as the degree of oxidation decreases with decreasing radial distance from the sun (Baedecker and Wasson, 1975).

Due to their high atomic number the Fe and Mn contents of rocks are detected by HH-EDXRF with high accuracy and precision (Zurfluh *et al.* 2011, Young *et al.* 2016). In this section, we demonstrate that: i) chemically and texturally heterogeneous samples although showing relatively large variations in Fe and Mn contents, have HH-EDXRF Fe/Mn ratios consistent with those of their own class, ii) Fe/Mn ratio obtained by HH-EDXRF together with other selected elements and/or element ratios can be routinely used to distinguish planetary basalts of differentiated bodies of the solar system.

Iron and Mn data from Millbillillie, Camel Donga, Nakhla, SaU 008, Chassigny and D'Orbigny are plotted in Figure 5. The figure shows that Fe and Mn contents determined from different slabs of

Camel Donga, D'Orbigny, Chassigny and Nakhla are nearly overlapping. This implies a textural and compositional homogeneity, at least at the HH-EDXRF spot size scale (8 mm). Camel Donga is, for instance, a monomict basaltic eucrite containing crystals and mm-sized lithic fragments set in a fine-grained matrix (Palme *et al.* 1988). D'Orbigny is an unshocked angrite mainly consisting of clinopyroxene, olivine and plagioclase with an overall subophitic texture (Mittlefehldt *et al.* 2002). Chassigny and Nakhla are almost mono-/bi-mineralic dunite and wherlite, respectively.

On the contrary, relatively larger spreads of results are observed for the eucrite Millbillillie and the shergottite SaU 008. This is in agreement with their petrographic and chemical data. Millbillillie is a mixture of basaltic portions, granulitic breccias and impact melts (Yamaguchi *et al.* 1994, Lauretta and Killgore, 2005). SaU 008 is a highly shocked porphyritic basalt containing large olivine set in a groundmass consisting of pyroxene and maskelynite and also several veins and pockets of shock melt (Zipfel, 2000). However, despite Millbillillie and SaU 008 are rather heterogeneous meteorites their HH-EDXRF Fe/Mn ratio plot on the Vesta and Martian trend line, respectively (Figure 5)

The average Fe/Mn ratios of five angrites, eight lunar meteorites, thirteen Martian meteorite and thirteen HED are plotted in Figure 6 together with the average Fe/Mn ratios of their own classes obtained from bulk compositional literature data. The average value of terrestrial basalts (IGBA database from Brändle and Nagy 1995) and the Fe/Mn ratios of twenty selected igneous rocks (basalts, basanites and diorites of Table S1) are also plotted for comparison.

Figure 6 shows that the large majority of the analysed samples plot within uncertainty in the variability range of their own class, given as 1 SD. There are, however, a few exceptions discussed below.

NWA 2999 is a unique angrite and has a HH-EDXRF Fe/Mn ratio of 120±4. This is higher than the angrites average value of 95±16 (Mittlefehldt and Lindstrom 1990, Yanai 1994, Mittlefehldt *et al.* 2002, Jambon *et al.* 2005, Gellissen *et al.* 2007, Shirai *et al.* 2009, Keil 2012). Although having an oxygen isotope composition characteristic of the angrite group ($\Delta^{17}O$ = -0.072±0.007, Greenwood et al. 2005), it has higher FeO and MgO contents relative to other angrites (Kuehner *et al.* 2006,

Gellissen *et al.* 2007). The measured Fe/Mn ratio is in very good agreement with the value of 130 reported by Gellissen *et al.* (2007) and as determined by WD-XRF.

The determined Fe/Mn ratio of Chassigny (~ 48±1) is higher than the average value of 40.2±4.5 reported for SNC meteorites (Dreibus *et al.* 1996, Warren *et al.* 1996, Lodders and Fegley 1998, Folco *et al.* 2000, Rubin *et al.* 2000, Zipfel *et al.* 2000, Barrat *et al.* 2002, Jambon *et al.* 2002, Anand *et al.* 2005, Barrat *et al.* 2006, Beck *et al.* 2006, Irving *et al.* 2011, Kuehner *et al.* 2011) This is not unexpected as Chassigny is the only Martian dunite. Papike *et al.* (2003) demonstrates that olivines have always higher Fe/Mn ratios than coexisting pyroxenes due to difference in M2 site occupancy. The HH-EDXRF measured Fe/Mn ratio is in full agreement with the value of 51 reported by Lodders and Fegley (1998) for Chassigny.

Zagami is a basaltic shergottite whose HH-EDXRF Fe/Mn ratio of 32.9±0.9 is lower than the average value of 40.2±4.5 reported for SNC meteorites (Figure 6). Zagami, is mineralogically and texturally heterogeneous and contains at least four different lithologies. Residual melts and impact melt lithologies are Fe-rich and show high Fe/Mn values (from 37.4 to 73.6, McCoy *et al.* 1992). This suggests that the Zagami sample (BM1966,54) analysed in this study did not contain a significant amount of Fe-rich melt. Moreover, our Fe/Mn ratio is indistinguishable within uncertainty from the bulk value of 33.2 determined by McCoy *et al.* (1992) on fused beads by EMPA and from the value of 33.1 obtained by Barrat *et al.* (2001) through ICP-AES.

The measured Fe/Mn ratios for the diogenites Shalka and Smara are 27.2±0.1 and 27.5±0.1, respectively. These values are lower than the average of 32.8±2.3 obtained for HED (Figure 6; Mittlefehldt 2015 and references therein), but comparable with whole rock Fe/Mn ratio of 28.1 determined by Kusuno *et al.* (2013) for Shalka and the 27.7 value reported by Barrat *et al.* (2003) for the matrix of Smara.

Figure 6 shows that the Fe/Mn ratios of the three lunar meteorites Dhofar 280 (91.2±13.5), Dhofar 961 (83.3±12.3) and Dhofar 908 (70.0±11.8) are, within uncertainty, in agreement with the average lunar value of 71±12. Note that the uncertainties in their Fe/Mn values are three times larger than

those obtained for the other lunar meteorites (Figure 6). This is likely due to their, very low Mn content close to LOD (Table 3), rather than to an internal heterogeneity.

Si and Ca/K values

The partial overlap of Fe/Mn values (Figure 6) between angrites and lunar meteorites as well as between HED and SNC implies that the HH-EDXRF Fe/Mn ratio alone should be treated with caution when used for preliminarily classification of these classes of achondrites. Herein, we suggest the use of additional and reliably measured elements or element ratios for such purposes. Figure 7a is a bulk Si vs Fe/Mn plot. In this plot angrites and lunar meteorites data can be well distinguished since angrites have much lower Si content (from 16 to 20.5 % m/m) than lunar meteorites (from 20.2 to 23.5 % m/m). The reason of this is that angrites are critically silica undersaturated rocks (Mittlefehldt *et al*., 2002), making the combined use of HH-EDXRF Si and Fe/Mn data very effective for their discrimination. Angra dos Reis is an exception because it has Si content (20.5 % m/m) comparable with those of lunar meteorites.

The compositional differences between HED and SNC meteorites could be better resolved by combining Fe/Mn with Ca/K ratio (Figure 7b). Calcium is a refractory lithophile element whose condensation temperature at $P=10^{-4}$ bar is 1634 K (Lodders and Fegley 1998), potassium is a moderately volatile lithophile element (50% condensation temperature = 1000 K; Lodders and Fegley (1998), and both enter the crystal lattice of plagioclase. Therefore, Ca/K can be used as a marker of moderately volatile element depletions of parent bodies in place of the more canonical Na/Al ratio, which cannot be determined with accuracy by HH-EDXRF. Figure 7b shows that HED are characterized by Ca/K roughly >100, while SNC plot approximately below this value. This is because HED meteorites are more depleted in volatile elements such as Na and K (see Figure 1 Mittlefehldt 2014). The wide range in Ca/K and Fe/Mn reflects variable modal abundance. For instance, within Martian meteorites the lowest Ca/K and the highest Fe/Mn ratio is observed for

more ultramafic rich end member (i.e. Chassigny), while a greater basaltic component, indicated by plagioclase, implies a higher Ca/K and lower Fe/Mn ratio (i.e. basaltic shergottites). In the HED class diogenites show the lowest Ca/K ratio, as they are mainly orthopyroxenite, while the eucrites have the highest Ca/K ratio because they are plagioclase-rich basalts or cumulates. It is worth mentioning, however, that terrestrial weathering in hot desert environments could result in calcium enrichment for Martian meteorites (e.g. Crozaz and Wadhwa 2001). Either hot desert secondary processes (e.g. Crozaz and Wadhwa 2001) or pristine features occurring in the HED parent body (e.g. Barrat et al. 2009) could lead to K enrichment in meteorites from Vesta. The overall effect is the occurrence of some minor overlapping in a Fe/Mn vs Ca/K space (Figure 7b).

HH-EDXRF measurement of Mg

The data reported in Table S1 and Figure 4 illustrates that some elements of geological relevance have sufficiently high analytical accuracy and precision to be useful for geochemical and cosmochemical classification. Among these, Mg is a key one. Due to its low atomic number, its determination by HH-EDXRF is generally considered unreliable (e.g., Young et al. 2016). Our experimental strategy of 150s total acquisition time (vs the total of 60 seconds used by Young et al. 2016) and the much larger number of studied samples has been specifically applied to address this issue. In Figure S1 (in Supporting Information) we compare the Mg content of the studied rock slabs with the terrestrial basalts analysed by Young *et al.* (2016). Both HH-EDXRF data are reported vs WD-XRF values. The tight clustering observed by our data, which plot close to the line of equality versus the greater dispersion of Young *et al.* (2016) data, suggesting lower accuracy and precision, is evident. This proves that our experimental and analytical approach makes the HH-EDXRF analysis of Mg fairly reliable and potentially able to disentangle ambiguities in the classification of both terrestrial and extraterrestrial rocks.

Fe/Mn values of fusion crusts

During atmospheric entry, meteoroids are decelerated from their initial velocity (approx. 12–18 km s^{-1}) to a terminal velocity approximately ranging from 1 to 10 km s^{-1}. Interaction with air increases their surface temperatures up to 2000–12000 K resulting in melting and ablation of the external layer (1 to 2 mm) of the meteorite. Such layer is called fusion crust.

Mineralogical and geochemical studies of meteorite fusion crusts (i.e. Genge and Grady, 1999) demonstrate that compositional differences with whole rock are the result of complex processes, which include evaporative loss of volatile elements. Hezel *et al.* (2015), show, in fact, that the fusion crust of ordinary chondrites is enriched in heavy Fe (^{56}Fe) and O isotopes (^{18}O) as a result of kinetic fractionation during evaporation.

After their fall on Earth meteorites are progressively altered through weathering. Alteration is proportional to the terrestrial age of the meteorites and its degree is function of environmental conditions. Crozaz and Wadhwa (2001), for example report the presence of clay minerals, terrestrial quartz and carbonate filling cracks, veins and mineral fractures in saharan shergottites. Terrestrial weathering in cold deserts can instead result in the dissolution of Ca-phosphates and formation of Fe-oxides and hydroxides (Crozaz et al. 2003). Therefore, caution should be exercised in the use of HH-EDXRF on meteorites showing clear signs of weathering.

In this section we report HH-EDXRF Fe and Mn abundances of the interior and fusion crust for 6 meteorite “falls” (5 SNCs and 1 HED) and 2 “finds” (the saharian DaG 669 and the antarctic Allan Hills 76005) (Table 3 and Figure 8). As all Fe and Mn Kα radiations are detected approximately within the first 100 to 500μm below the sample surface (Potts, 1992), we are confident that the measured Fe and Mn values represent the actual fusion crust values. The composition of fusion crusts for 5 HEDs and one SNC obtained by Genge and Grady (1999) and Gnos et al. (2002) through EMPA have been plotted as well. In Figure 8 best-fit line passing through bulk literature data of 74 HEDs and 55 SNCs, together with 68% and 95% confidence interval are also reported. Figure 8a shows that the fusion crust of diogenites and howardites are consistently depleted in Fe

and Mn respect to the host meteorite. The fusion crust of the eucrites is, instead, almost identical to the interior. The only exception, possibly reflecting some internal heterogeneity or a weak alteration of the crust is the polymict eucrite ALH 76005 whose fusion crust has lower HH-EDXRF Fe and Mn content than that of the host meteorite. However, the HH-EDXRF Fe/Mn ratio of the HEDs fusion crusts always shows values typical of meteorites coming from Vesta. Genge and Grady (1999) observe that the melted crusts of howardites and diogenites have larger variations from bulk meteorite than eucrites. Moreover, contrary to chondrites, they describe fusion crusts of HEDs as mainly glassy, rarely containing relic grains or metal/sulphide droplets.

In terms of Fe and Mn, Figure 8b shows that the fusion crusts of SNCs are compositionally indistinguishable from the bulk meteorites and fall in the field of meteorites coming from Mars. To our knowledge there are no studies on the textural characterization of SNCs fusion crusts. However, from the data plotted in Figure 8b we infer that the fusion crust of SNCs are as homogeneous as those of eucrites and that little (if any) fractionation of Fe and Mn occurred during the atmospheric entry.

Combining HH-EDXRF analyses with magnetic susceptibility measurements.

Preliminary classification of meteorites can also be obtained by measurements of their magnetic susceptibility (Rochette et al. 2003, 2004). The magnetic susceptibility of rocks is function of their magnetic minerals content and measures the ability of the material to acquire magnetization when placed in a magnetic field. Because of its simplicity, this non-destructive method is helpful, in the discrimination of meteorites from terrestrial stones as well as in distinguishing stony meteorites, which are the most abundant meteorites in our collections (95% of the total) into two major categories, the achondrites from the chondrites. As such, the magnetic method is a powerful tool for curatorial purposes providing an accurate and efficient means for first classification of meteorites (Rochette *et al.* 2003, Rochette *et al.* 2004, Rochette *et al.* 2008, Rochette *et al.* 2009). Furthermore,

Gattacceca et al. (2004) developed a method for the measurements of magnetic susceptibility in meteorites through a pocket probe, subsequently tested directly in the field during the search for meteorites within the framework of the Programma Nazionale delle Ricerche in Antartide (PNRA) (Folco et al. 2006).

Although enabling discrimination of the rare differentiated achondrites from the more common chondrites, a limitation of the magnetic method is the overlap in the magnetic susceptibility values of the different classes of this group of important meteorites (e.g., HEDs, lunar meteorites, SNCs, and angrites; see Figure 1 in Folco et al. 2006 and Figure 2 in Rochette et al. 2009). Figure 9 shows how the combination of HH-EDXRF analyses and magnetic method can provide an efficient tool for identification and classification of differentiated meteorites.

HH-EDXRF Fe/Mn ratios of some analyzed achondrites versus the magnetic susceptibility values of the same meteorites (reported as Logχ) taken from literature (Rochette *et al.* 2009, Rochette *et al.* 2010, Collareta *et al.* 2016). The compositional ranges for chondritic meteorites are also shown for comparison. There is a gap in the distribution of the Logχ data at about 3.8 documenting the power of the magnetic method in discriminating chondrites from achondrites. The Fe/Mn ratios of HEDs, SNCs, angrites and lunar meteorites obtained by HH-EDXRF are reasonably well distinguished (Figures 6, 7 and 9) while partial overlap exists with ordinary chondrites. An accurate first classification of an achondrite can thus be obtained by its identification at the group level through magnetic susceptibility measurements and its classification to the class level by means of HH-EDXRF analyses.

Figure 9 thus highlights that the combined use of HH-EDXRF and magnetic susceptibility measurements can be very effective for initial meteorite classification. This is particularly useful when surveying large collections, like those recovered by meteorite search expedition from hot and cold deserts, to establish curatorial priorities. Both devices are technically simple to use and very practical due to their portability and limited energy consumption. The use of HH-EDXRF and magnetic susceptibility probe have become part of the field curation equipment of the Italian PNRA

Antarctic meteorite search campaigns and, by extension, it could be an important addition to the instrumentations designed for planetary surface exploration missions.

Conclusions

Our study focused on the development of a proper analytical protocol for discriminating different groups of achondritic meteorites by HH-EDXRF analysis.

We have demonstrated that:

i) HH-EDXRF is a very stable instrument, suitable to get robust data for elements heavier than Na in mafic and ultramafic rocks (terrestrial and extraterrestrial).

ii) The combination of an SDD detector, the acquisition times of 150 s and a careful calibration obtained through the analyses of a wide set of igneous rocks highly improved the analytical precision and accuracy of the data, making even the measurement of Mg sufficiently reliable.

iii) Fe and Mn are routinely obtained by HH-EDXRF allowing classification of differentiated stony meteorites and thus planetary basalts based on the bulk Fe/Mn key element ratio.

iv) The combination of the bulk Fe/Mn ratio with the concentration of other elements or element ratios can help to improve discrimination between different classes of achondrites where some overlap in Fe/Mn ratio exists. For instance, we demonstrate that Si and Ca/K against Fe/Mn can resolve the partial Fe/Mn overlap between lunar meteorites and angrites and between HEDs and SNCs, respectively.

v) Despite the complexity of the processes related to the atmospheric entry of meteoroids, Fe/Mn values of achondritic meteorite fusion crust are indistinguishable from those of the interior. This implies that “rough and ready” Fe/Mn measurements of the fusion crusts of achondrites could be sufficient for preliminary screening and identification of their parentage.

vi) Due to its principal characteristics and capabilities (portability, and rapid, non-destructive, accurate analyses), HH-EDXRF thus proves to be a valuable and practical tool for curatorial

purposes. It can be used to: (a) confirm/verify the extraterrestrial origin of rock samples; (b) provides a preliminary chemical classification of new meteorite finds; (c) identify mislabelled/unlabelled specimens in museums and private collections.

vii) The combined use of a HH-EDXRF and of a magnetic susceptibility probe is ideal both in the laboratory and in the field to discriminate achondritic from chondritic meteorites and for preliminary classification of HEDs, lunar meteorites, SNCs and angrites.

Acknowledgments

This work is supported by the Italian Programma Nazionale delle Ricerche in Antartide (PNRA), project 'Meteoriti Antartiche'. We thank Caroline Smith (Natural History Museum, London, UK), Sonia Sandroni (MNA-SI, Italy) and Romano Serra (Museo del Cielo e della Terra, San Giovanni in Persiceto, Italy) for providing achondrite samples. We thank two anonymous reviewers for constructive reviews and Joint Editor-in-Chief Mary Horan for editorial handling and useful comments.

References

Anand, **M.**, **Taylor**, **L.A.**, **Misra**, **K.C.**, **Demidova**, **S.I.** and **Nazarov**, **M.A.** (2003). KREEPy lunar meteorite Dhofar 287A: A new lunar mare basalt. **Meteoritics & Planetary Science**, **38**, 485–499.

Anand, **M.**, **Williams**, **C.T.**, **Russell**, **S.S.**, **Jones**, **G.**, **James**, **S.** and **Grady**, **M.M.** (2005). Petrology and geochemistry of nakhlite MIL 03346: A new Martian meteorite from Antarctica. **36th Lunar and Planetary Science Conference**, Abstract 1639.

Anand, **M.**, **Taylor**, **L.A.**, **Floss**, **C.**, **Neal**, **C.R.**, **Terada**, **K.** and **Tanikawa**, **S. (2006)**. Petrology and geochemistry of LaPaz Icefield 02205: A new unique low-Ti mare-basalt meteorite. **Geochimica et Cosmochimica Acta**, **70**, 246–264.

Anand, **M.**, **Taylor**, **L.A.**, **Misra**, **K.C.**, **Demidova**, **S.I.** and **Nazarov**, **M.A. (2003)**. KREEPy

lunar meteorite Dhofar 287A: A new lunar mare basalt. **Meteoritics & Planetary Science**, **38**, 485–499.

Anand, **M.**, **Williams**, **C.T.**, **Russell**, **S.S.**, **Jones**, **G.**, **James**, **S.** and **Grady**, **M.M. (2005)**. Petrology and geochemistry of nakhlite MIL 03346: A new Martian meteorite from Antarctica. **36th Lunar and Planetary Science Conference**, Abstract 1639.

Baedecker, **P.A.** and **Wasson**, **J.T. (1975)**. Elemental fractionations among enstatite chondrites. **Geochimica et Cosmochimica Acta**, **39**, 735–765.

Barrat, **J.-A.**, **Benoit**, **M.** and **Cotten**, **J. (2006)**. Bulk Chemistry of the Nakhlite Miller Range 03346 (MIL 03346). **37th Lunar and Planetary Science Conference,** Abstract 1569.

Barrat, **J.-A.**, **Blichert-Toft**, **J.**, **Nesbitt**, **R.W.** and **Keller**, **F. (2001)**. Bulk chemistry of Saharan shergottite Dar al Gani 476. **Meteoritics & Planetary Science**, **36**, 23–29.

Barrat, **J.A.**, **Gillet**, **P.**, **Sautter**, **V.**, **Jambon**, **A.**, **Javoy**, **M.**, **Gopel**, **C.**, **Lesourd**, **M.**, **Keller**, **F.** and **Petit**, **E. (2002)**. Petrology and chemistry of the basaltic shergottite North West Africa 480. **Meteoritics & Planetary Science**, **37**, 487–499.

Barrat, **J.A.**, **Jambon**, **A.**, **Bohn**, **M.**, **Blichert-Toft**, **J.**, **Sautter**, **V.**, **Göpel**, **C.**, **Gillet**, **P.**, **Boudouma**, **O.** and **Keller**, **F. (2003)**. Petrology and geochemistry of the unbrecciated achondrite Northwest Africa 1240 (NWA 1240): An HED parent body impact melt. **Geochimica et Cosmochimica Acta**, **67**, 3959–3970.

Barrat J.-A. Yamaguchi A. Greenwood R. C. Bollinger C. Bohn M. and **Franchi I. A.** 2009. Trace element geochemistry of K-rich impact spherules from howardites. *Geochimica et Cosmochimica Acta* 73: 5944–5958.

Beck, **P.**, **Barrat**, **J.A.**, **Gillet**, **P.**, **Wadhwa**, **M.**, **Franchi**, **I.A.**, **Greenwood**, **R.C.**, **Bohn**, **M.**, **Cotten**, **J.**, **van de Moortèle**, **B.** and **Reynard**, **B. (2006)**. Petrography and geochemistry of the chassignite Northwest Africa 2737 (NWA 2737). **Geochimica et Cosmochimica Acta**, **70**, 2127–2139.

Bischoff, **A.**, **Weber**, **D.**, **Clayton**, **R.N.**, **Faestermann**, **T.**, **Franchi**, **I.A.**, **Herpers**, **U.**, **Knie**, **K.**, **Korschinek**, **G.**, **Kubik**, **P.W.** and **Mayeda**, **T.K. (1998)**. Petrology, chemistry, and isotopic compositions of the lunar highland regolith breccia Dar al Gani 262. **Meteoritics & Planetary Science**, **33**, 1243–1257.

Bouvier, **A.** and **Wadhwa**, **M. (2010)**. The age of the Solar System redefined by the oldest Pb--Pb age of a meteoritic inclusion. **Nature Geoscience**, **3**, 637–641.

Brändle, **J.L.** and **Nagy**, **G. (1995)**. The state of the 5th version of IGBA: Igneous Petrological Data Base. **Computers & Geosciences**, **21**, 425–432.

Burbine, **T.H.**, **Mccoy**, **T.J.** and **Bin-Zel**, **R.P. (2001)**. Spectra of angrites and possible parent bodies. **32nd Lunar and Planetary Science Conference,** Abstract 1857.

Burbine, **T.H.**, **McCoy**, **T.J.**, **Hinrichs**, **J.L.** and **Lucey**, **P.G. (2006)**. Spectral properties of angrites. **Meteoritics & Planetary Science**, **41**, 1139–1145.

Cahill, **J.T.S.**, **Lucey**, **P.G.** and **Wieczorek**, **M.A. (2009)**. Compositional variations of the lunar crust: Results from radiative transfer modeling of central peak spectra. **Journal of Geophysical Research**, **114**, E09001.

Cameron, **M.** and **Papike**, **J.J. (1981)**. Structural and chemical variations in pyroxenes. **American Mineralogist**, **66**, 1–50.

Clayton, **R.N.** and **Mayeda**, **T.K. (1996)**. Oxygen isotope studies of achondrites. **Geochimica et Cosmochimica Acta**, **60**, 1999–2017.

Collareta, **A.**, **D'Orazio**, **M.**, **Gemelli**, **M.**, **Pack**, **A.** and **Folco**, **L. (2016)**. High crustal diversity preserved in the lunar meteorite Mount DeWitt 12007 (Victoria Land, Antarctica). **Meteoritics & Planetary Science**, **51, 351–371**.

Comelli, **D.**, **D'orazio**, **M.**, **Folco**, **L.**, **El-Halwagy**, **M.**, **Frizzi**, **T.**, **Alberti**, **R.**, **Capogrosso**, **V.**, **Elnaggar**, **A.**, **Hassan**, **H.**, **Nevin**, **A.**, **Porcelli**, **F.**, **Rashed**, **M.G.** and **Valentini**, **G. (2016)**. The meteoritic origin of Tutankhamun's iron dagger blade. **Meteoritics & Planetary Science**, **51**, 1301–1309.

Consolmagno, **G.J.** and **Drake**, **M.J. (1977)**. Composition and evolution of the eucrite parent body: evidence from rare earth elements. **Geochimica et Cosmochimica Acta**, **41**, 1271–1282.

Crozaz G. Floss C. and **Wadhwa M.** 2003. Chemical alteration and REE mobilization in meteorites from hot and cold deserts. *Geochimica et Cosmochimica Acta* 67.

Crozaz G. and **Wadhwa M.** 2001. The terrestrial alteration of saharan shergottites dar al gani 476 and 489: a case study of weathering in a hot desert environment. *Geochimica et Cosmochimica Acta* 65: 971–977.

Demidova, **S.I.**, **Nazarov**, **M.A.**, **Anand**, **A.** and **Taylor**, **L.A. (2003)**. Lunar regolith breccia Dhofar 287B: A record of lunar volcanism. **Meteoritics & Planetary Science**, **38**, 501–514.

Demidova, **S.I.**, **Nazarov**, **M.A.**, **Lorenz**, **C.A.**, **Kurat**, **G.**, **Brandstätter**, **F.** and **Ntaflos**, **T. (2007)**. Chemical composition of lunar meteorites and the lunar crust. **Petrology**, **15**, 386–407.

Dreibus, **G.**, **Spettel**, **B.**, **Wlotzka**, **F.**, **Schultz**, **L.**, **Weber**, **H.W.**, **Jochum**, **K.P.** and **Wanke**, **H. (1996)**. QUE94201: an Unusual Martian Basalt. **Meteoritics & Planetary Science, 31, A39**, **31**.

Fagan, **T.J.**, **Taylor**, **G.J.**, **Keil**, **K.**, **Bunch**, **T.E.**, **Wittke**, **J.H.**, **Korotev**, **R.L.**, **Jolliff**, **B.L.**, **Gillis**, **J.J.**, **Haskin**, **L. a**, **Jarosewich**, **E.**, **Clayton**, **R.N.**, **Mayeda**, **T.K.**, **Fernandes**, **V. a**, **Burgess**, **R.**, **Turner**, **G.**, **Eugster**, **O.** and **Lorenzetti**, **S. (2002)**. Northwest Africa 032: Product of lunar volcanism. **Meteoritics & Planetary Science**, **37**, 371–394.

Fagan, **T.J.**, **Taylor**, **G.J.**, **Keil**, **K.**, **Hicks**, **T.L.**, **Killgore**, **M.**, **Bunch**, **T.E.**, **Wittke**, **J.H.**, **Mittlefehldt**, **D.W.**, **Clayton**, **R.N.**, **Mayeda**, **T.K.**, **Eugster**, **O.**, **Lorenzetti**, **S.** and **Norman**, **M.D. (2003)**. Northwest Africa 773: Lunar origin and iron-enrichment trend. **Meteoritics & Planetary Science**, **38**, 529–554.

Folco, **L.**, **Franchi**, **I.A.**, **D'Orazio**, **M.**, **Rocchi**, **S.** and **Schultz**, **L. (2000)**. A new martian meteorite from the Sahara: The shergottite Dar al Gani 489. **Meteoritics & Planetary Science**, **35**, 827–839.

Franchi, **I.A.**, **Wright**, **I.P.**, **Sexton**, **A.S.** and **Pillinger**, **C.T. (1999)**. The oxygen-isotopic composition of Earth and Mars. **Meteoritics & Planetary Science**, **34**, 657–661.

Gattacceca, **J.**, **Eisenlohr**, **P.** and **Rochette**, **P. (2004)**. Calibration of in situ magnetic susceptibility measurements. **Geophysical Journal International**, **158**, 42–49.

Gellissen, **M.**, **Palme**, **H.**, **Korotev**, **R.L.** and **Irving**, **A.J. (2007)**. NWA 2999, a unique angrite with a large chondritic component. **38th Lunar and Planetary Science Conference,** Abstract 1612.

Gemelli, **M.**, **D'Orazio**, **M.** and **Folco**, **L. (2015)**. Chemical Analysis of Iron Meteorites Using a Hand-Held X-Ray Fluorescence Spectrometer. **Geostandards and Geoanalytical Research**, **39**, 55–69.

Genge, **M.J.** and **Grady**, **M.M. (1999)**. The fusion crusts of stony meteorites: Implications for the atmospheric reprocessing of extraterrestrial materials. **Meteoritics & Planetary Science**, **34**, 341–

356.

Gillis, **J.J.**, **Jolliff**, **B.L.** and **Korotev**, **R.L. (2004)**. Lunar surface geochemistry: Global concentrations of Th, K, and FeO as derived from lunar prospector and Clementine data. **Geochimica et Cosmochimica Acta**, **68**, 3791–3805.

Gnos, **E.**, **Hofmann**, **B.**, **Franchi**, **I.A.**, **Al-Kathiri**, **A.**, **Huser**, **M.** and **Moser**, **L. (2002)**. Sayh al Uhaymir 094: A new martian meteorite from the Oman desert. **Meteoritics & Planetary Science**, **37**, 835–854.

Goodrich, **C.A.** and **Delaney**, **J.S. (2000)**. Fe/Mg-Fe-Mn relations of meteorites and primary heterogeneity of primitive achondrite parent bodies. **Geochimica et Cosmochimica Acta**, **64**, 149–160.

Greenwood, **R.C.**, **Franchi**, **I.A.**, **Jambon**, **A.** and **Buchanan**, **P.C. (2005)**. Widespread magma oceans on asteroidal bodies in the early Solar System. **Nature**, **435**, 916–918.

Greshake, **A.**, **Irving**, **A.J.**, **Kuehner**, **S.M.**, **Korotev**, **R.L.**, **Gellissen**, **M.** and **Palme**, **H. (2008)**. Northwest Africa 4898: a new high-alumina mare basalt from the moon. **39th Lunar and Planetary Science**, Abstract 1631.

Halliday, **A.N.** and **Kleine**, **T. (2006)**. Meteorites and Planetary Accrection and Differentiation. **In Lauretta, D.S. and McSween, H.Y., (eds), Meteorites and Early Solar System II**. **University of Arizona Press**, 775–801.

Haloda, **J.**, **Tycova**, **P.**, **Jakes**, **P.**, **Gabzdyl**, **P.** and **Kosler**, **J. (2006)**. Lunar meteorite Northeast Africa 003-b: a new lunar mare basaltic breccia. **37th Lunar and Planetary Science**, Abstract 2311.

Haloda, **J.**, **Týcová**, **P.**, **Korotev**, **R.L.**, **Fernandes**, **V.A.**, **Burgess**, **R.**, **Thöni**, **M.**, **Jelenc**, **M.**, **Jakeš**, **P.**, **Gabzdyl**, **P.** and **Košler**, **J. (2009)**. Petrology, geochemistry, and age of low-Ti mare-basalt meteorite Northeast Africa 003-A: A possible member of the Apollo 15 mare basaltic suite. **Geochimica et Cosmochimica Acta**, **73**, 3450–3470.

Hezel, **D.C.**, **Poole**, **G.M.**, **Hoyes**, **J.**, **Coles**, **B.J.**, **Unsworth**, **C.**, **Albrecht**, **N.**, **Smith**, **C.**, **Rehkämper**, **M.**, **Pack**, **A.**, **Genge**, **M.** and **Russell**, **S.S. (2015)**. Fe and O isotope composition of meteorite fusion crusts: Possible natural analogues to chondrule formation? **Meteoritics & Planetary Science**, **50**, 229–242.

Irving, **A.J.**, **Kuehner**, **S.M.** and **Rumble**, **D. (2006)**. A Fresh Plutonic Igneous Angrite Containing Grain Boundary Glass From Tamassint, Northwest Africa. **American Geophysical Union, Fall Meeting 2006,** Abstract **P51E-1245**.

Irving, **A.J.**, **Kuehner**, **S.M.**, **Rumble**, **D.**, **Bunch**, **T.E.** and **Wittke**, **J.H. (2005)**. Unique Angrite NWA 2999: The Case For Samples From Mercury. **American Geophysical Union, Fall Meeting 2005,** Abstract **P51A-0898**.

Irving, **J.**, **Bunch**, **T.E.**, **Kuehner**, **S.M.**, **K Herd**, **C.D.**, **Gellissen**, **M.**, **Lapen**, **T.J.**, **Rumble**, **D.** and **Pitt**, **D. (2011)**. Petrologic, elemental and isotopic characterization of shock-melted, enriched ultramafic poikilitic shergottite Northwest Africa 6342. **42nd Lunar and Planetary Science Conference,** Abstract 1612.

Jambon, **A.**, **Barrat**, **J.A.**, **Boudouma**, **O.**, **Fonteilles**, **M.**, **Badia**, **D.**, **Göpel**, **C.** and **Bohn**, **M. (2005)**. Mineralogy and petrology of the angrite Northwest Africa 1296. **Meteoritics & Planetary Science**, **40 (3)**, 361–375.

Jambon, **A.**, **Barrat**, **J.**, **Sautter**, **V.**, **Gillet**, **P.**, **Gopel**, **C.**, **Javoy**, **M.**, **Joron**, **J.L.** and **Lesourd**, **M. (2002)**. the basaltic shergottite northwest Africa 856: Petrology and chemistry. **Meteoritics & Planetary Science**, **37**, 1147–1164.

Jolliff, **B.L.**, **Gillis**, **J.J.**, **Haskin**, **L.A.**, **Korotev**, **R.L.** and **Wieczorek**, **M.A. (2000)**. Major lunar crustal terranes: Surface expressions and crust-mantle origins. **Journal of Geophysical Research: Planets**, **105**, 4197–4216.

Joy, **K.H.**, **Crawford**, **I.A.**, **Anand**, **M.**, **Greenwood**, **R.C.**, **Franchi**, **I.A.** and **Russell**, **S.S. (2008)**. The petrology and geochemistry of Miller Range 05035: A new lunar gabbroic meteorite. **Geochimica et Cosmochimica Acta**, **72**, 3822–3844.

Joy, **K.H.**, **Crawford**, **I.A.**, **Downes**, **H.**, **Russell**, **S.S.** and **Kearsley**, **A.T. (2006)**. A petrological, mineralogical, and chemical analysis of the lunar mare basalt meteorite LaPaz Icefield 02205, 02224, and 02226. **Meteoritics & Planetary Science**, **41**, 1003–1025.

Joy, **K.H.**, **Crawford**, **I.A.**, **Russell**, **S.S.** and **Kearsley**, **A.T. (2010)**. Lunar meteorite regolith breccias: An in situ study of impact melt composition using LA-ICP-MS with implications for the composition of the lunar crust. **Meteoritics & Planetary Science**, **45**, 917–946.

Kalnicky, **D.J.** and **Singhvi**, **R. (2001)**. Field portable XRF analysis of environmental samples. **Journal of hazardous materials**, **83**, 93–122.

Keil, **K. (2012)**. Angrites, a small but diverse suite of ancient, silica-undersaturated volcanic-plutonic mafic meteorites, and the history of their parent asteroid. **Chemie der Erde - Geochemistry**, **72**, 191–218.

Kenna, **T.C.**, **Nitsche**, **F.O.**, **Herron**, **M.M.**, **Mailloux**, **B.J.**, **Peteet**, **D.**, **Sritrairat**, **S.**, **Sands**, **E.** and **Baumgarten**, **J. (2011)**. Evaluation and calibration of a Field Portable X-Ray Fluorescence spectrometer for quantitative analysis of siliciclastic soils and sediments. **Journal of Analytical Atomic Spectrometry**, **26**, 395–405.

Kirtay, **V.J.**, **Kellum**, **J.H.** and **Apitz**, **S.E. (1998)**. Field-portable X-ray Fluorescence Spectrometry for metals in marine sediments: Results from multiple sites. **Water Science and Technology**, **37**, 141–148.

Kobayashi, **S.**, **Hasebe**, **N.**, **Shibamura**, **E.**, **Okudaira**, **O.**, **Kobayashi**, **M.**, **Yamashita**, **N.**, **Karouji**, **Y.**, **Hareyama**, **M.**, **Hayatsu**, **K.**, **d'Uston**, **C.**, **Maurice**, **S.**, **Gasnault**, **O.**, **Forni**, **O.**, **Diez**, **B.**, **Reedy**, **R.C.** and **Kim**, **K.J. (2010)**. Determining the Absolute Abundances of Natural Radioactive Elements on the Lunar Surface by the Kaguya Gamma-ray Spectrometer. **Space Science Reviews**, **154**, 193–218.

Kohout, **T.**, **Kletetschka**, **G.**, **Kobr**, **M.**, **Pruner**, **P.** and **Wasilewski**, **P.J. (2004)**. The influence of terrestrial processes on meteorite magnetic records. **Physics and Chemistry of the Earth, Parts A/B/C**, **29**, 885–897.

Korotev, **R.L. (2005)**. Lunar geochemistry as told by lunar meteorites. **Chemie der Erde - Geochemistry**, **65**, 297–346.

Korotev, **R.L.**, **Jolliff**, **B.L.**, **Zeigler**, **R.A.**, **Gillis**, **J.J.** and **Haskin**, **L.A. (2003)**. Feldspathic lunar meteorites and their implications for compositional remote sensing of the lunar surface and the composition of the lunar crust. **Geochimica et Cosmochimica Acta**, **67**, 4895–4923.

Korotev, **R.L.**, **Zeigler**, **R.A.**, **Jolliff**, **B.L.**, **Irving**, **A.J.** and **Bunch**, **T.E. (2009)**. Compositional and lithological diversity among brecciated lunar meteorites of intermediate iron concentration. **Meteoritics & Planetary Science Archives**, **44**, 1287–1322.

Kuehner, **S.M.** and **Irving**, **A.J. (2007)**. Primary Ferric Iron-Bearing Rhönite in Plutonic Igneous Angrite NWA 4590: Implications for Redox Conditions on the Angrite Parent Body. **American Geophysical Union, Fall Meeting 2007,** Abstract P41A-0219.

Kuehner, **S.M.**, **Irving**, **A.J.**, **Bunch**, **T.E.**, **Wittke**, **J.H.**, **Hupé**, **G.M.** and **Hupé**, **A.C. (2006)**.

Coronas and Symplectites in Plutonic Angrite NWA 2999 and Implications for Mercury as the Angrite Parent Body. **37th Lunar and Planetary Science Conference**, Abstract #1344.

Kuehner, **S.M.**, **Irving**, **A.J.**, **Herd**, **C.D.K.**, **Gellissen**, **M.**, **Lapen**, **T.J.** and **Rumble**, **D. (2011)**. Pristine olivine-phyric shergottite Northwest Africa 6162: a primitive magma with accumulated crystals derived from depleted martian mantle. **42nd Lunar and Planetary Science Conference,** Abstract 1610.

Kusuno, **H.**, **Fukuoka**, **T.** and **Matsuzaki**, **H. (2013)**. Simple relationship between 26 Al production rate and major elemental composition of meteorite samples. **Geochemical Journal, 47**, 83–88.

Lauretta, **D.S. and Killgore**, **M. (2005)**. A color atlas of meteorites in thin section. **Golden Retriever Publications**, 301pp.

Lawrence, **D.J.**, **Puetter**, **R.C.**, **Elphic**, **R.C.**, **Feldman**, **W.C.**, **Hagerty**, **J.J.**, **Prettyman**, **T.H.** and **Spudis**, **P.D. (2007)**. Global spatial deconvolution of Lunar Prospector Th abundances. **Geophysical Research Letters**, **34**, L03201.

Lindstrom, **M.M.**, **Schwarz**, **C.**, **Score**, **R.** and **Masons**, **B. (1991)**. MacAlpine Hills 88104 and 88105 lunar highland meteorites: General description and consortium overview. **Geochimica et Cosmochimica Acta**, **55**, 2999–3007.

Lindstrom, **M.M.**, **Treiman**, **A.H.** and **Mittlefehldt**, **D.W. (1994)**. Pigeonholing planetary meteorites: the lessons of misclassification of eet 87521 and alh 84001. **25th Lunar and Planetary Science**, Abstract 797.

Liritzis, **I.** and **Zacharias**, **N. (2011)**. Portable XRF of Archaeological Artifacts: Current Research, Potentials and Limitations. **In: Shackley, M.S. (ed), X-Ray Fluorescence Spectrometry (XRF) in Geoarchaeology. Springer (New York),** 109–142.

Liu, **Y.**, **Floss**, **C.**, **Day**, **J.M.D.**, **Hill**, **E.** and **Taylor**, **L.A. (2009)**. Petrogenesis of lunar mare basalt meteorite Miller Range 05035. **Meteoritics & Planetary Science**, **44**, 261–284.

Lodders, **K.** and **Fegley**, **B. (1998)**. The planetary scientist's companion. **Oxford University Press,** 371pp.

Macke, **R.J.**, **Britt**, **D.T.** and **Consolmagno**, **G.J. (2011)**. Density, porosity, and magnetic

susceptibility of achondritic meteorites. **Meteoritics & Planetary Science**, **46**, 311–326.

McCarthy, **T.S.**, **Erlank**, **A.J.** and **Willis**, **J.P. (1973)**. On the origin of eucrites and diogenites. **Earth and Planetary Science Letters**, **18**, 433–442.

McCord, **T.B.**, **Adams**, **J.B.** and **Johnson**, **T. V. (1970)**. Asteroid Vesta: Spectral Reflectivity and Compositional Implications. **Science**, **168**, 1445–1447.

McCoy, **T.J.**, **Corrigan**, **C.M.** and **Herd**, **C.D.K. (2011)**. Combining meteorites and missions to explore Mars. **Proceedings of the National Accademy of Sciences of the USA**, **108**, 19159–19164.

McCoy, **T.J.**, **Taylor**, **G.J.** and **Keil**, **K. (1992)**. Zagami: Product of a two-stage magmatic history. **Geochimica et Cosmochimica Acta**, **56**, 3571–3582.

McSween, **H.Y. (1994)**. What we have learned about Mars from SNC meteorites. **Meteoritics**, **29**, 757–779.

Mészáros, **M.**, **Hofmann**, **B.A.**, **Lanari**, **P.**, **Korotev**, **R.L.**, **Gnos**, **E.**, **Greber**, **N.D.**, **Leya**, **I.**, **Greenwood**, **R.C.**, **Jull**, **A.J.T.**, **Al-Wagdani**, **K.**, **Mahjoub**, **A.**, **Al-Solami**, **A.A.** and **Habibullah**, **S.N. (2016)**. Petrology and geochemistry of feldspathic impact-melt breccia Abar al' Uj 012, the first lunar meteorite from Saudi Arabia. **Meteoritics & Planetary Science**, **51**, 1830–1848.

Mittlefehldt, **D.W. (2014)**. Achondrites. **In Holland H. D. and Turekian K. K. (eds.), Treatise on Geochemistry (Second Edition), Elsevier (Oxford),** 235–266.

Mittlefehldt, **D.W. (2015)**. Asteroid (4) Vesta: I. The howardite-eucrite-diogenite (HED) clan of meteorites. **Chemie der Erde - Geochemistry**, **75**, 155–183.

Mittlefehldt, **D.W. (1979)**. Petrographic and chemical characterization of igneous lithic clasts from mesosiderites and howardites and comparison with eucrites and diogenites. **Geochimica et Cosmochimica Acta**, **43**, 1917–1935.

Mittlefehldt, **D.W.**, **Goodrich**, **C.A.**, **Kracher**, **A.** and **McCoy**, **T.J. (1998)**. Non-Chondritic Meteorites from Asteroidal Bodies. **In: Papike, J.J. (ed.) Planetary Materials. Reviews in Mineralogy**, 1–196.

Mittlefehldt, **D.W.**, **Killgore**, **M.** and **Lee**, **M.T.M.T. (2002)**. Petrology and geochemistry of D'Orbigny, geochemistry of Sahara 99555, and the origin of angrites. **Meteoritics & Planetary Science**, **37**, 345–369.

Mittlefehldt, **D.W.** and **Lindstrom**, **M.M. (1990)**. Geochemistry and genesis of the angrites. **Geochimica et Cosmochimica Acta**, **54**, 3209–3218.

Nittler, **L.R.**, **McCoy**, **T.J.**, **Clark**, **P.E.**, **Murphy**, **M.E.**, **Trombka**, **J.I.** and **Jarosewich**, **E. (2004)**. Bulk element compositions of meteorites: A guide for interpreting remote-sensing geochemical measurements of planets and asteroids. **Antartic Meteorite Research, 17,** 233-253.

Nyquist, **L.**, **Bogard**, **D.**, **Yamaguchi**, **A.**, **Shih**, **C.-Y.**, **Karouji**, **Y.**, **Ebihara**, **M.**, **Reese**, **Y.**, **Garrison**, **D.**, **McKay**, **G.** and **Takeda**, **H. (2006)**. Feldspathic clasts in Yamato-86032: Remnants of the lunar crust with implications for its formation and impact history. **Geochimica et Cosmochimica Acta**, **70**, 5990–6015.

Ohtake, **M.**, **Matsunaga**, **T.**, **Haruyama**, **J.**, **Yokota**, **Y.**, **Morota**, **T.**, **Honda**, **C.**, **Ogawa**, **Y.**, **Torii**, **M.**, **Miyamoto**, **H.**, **Arai**, **T.**, **Hirata**, **N.**, **Iwasaki**, **A.**, **Nakamura**, **R.**, **Hiroi**, **T.**, **Sugihara**, **T.**, **Takeda**, **H.**, **Otake**, **H.**, **Pieters**, **C.M.**, **Saiki**, **K.**, **Kitazato**, **K.**, **Abe**, **M.**, **Asada**, **N.**, **Demura**, **H.**, **Yamaguchi**, **Y.**, **Sasaki**, **S.**, **Kodama**, **S.**, **Terazono**, **J.**, **Shirao**, **M.**, **Yamaji**, **A.**, **Minami**, **S.**, **Akiyama**, **H.** and **Josset**, **J.-L. (2009)**. The global distribution of pure anorthosite on the Moon. **Nature**, **461**, 236–240.

Ohtake, **M.**, **Takeda**, **H.**, **Matsunaga**, **T.**, **Yokota**, **Y.**, **Haruyama**, **J.**, **Morota**, **T.**, **Yamamoto**, **S.**, **Ogawa**, **Y.**, **Hiroi**, **T.**, **Karouji**, **Y.**, **Saiki**, **K.** and **Lucey**, **P.G. (2012)**. Asymmetric crustal growth on the Moon indicated by primitive farside highland materials. **Nature Geoscience**, **5**, 384–388.

Palme, **H.**, **Wlotzka**, **F.**, **Spettel**, **B.**, **Dreibus**, **G.** and **Weber**, **H. (1988)**. Camel Donga: A Eucrite with High Metal Content. **Meteoritics**, **23**, 49–57.

Papike, **J.J.**, **Karner**, **J.M.** and **Shearer**, **C.K. (2003)**. Determination of planetary basal parentage: A simple technique using the electron microprobe. **American Mineralogist**, **88**, 469–472.

Potts P.J. (1987). Chapter 8: X-ray fluorescence analysis: principles and practice of wavelength dispersive spectrometry. **In: A handbook of silicate rock analysis.** Blackie (Glasgow and London), 226–285.

Potts, **P.J.** and **West**, **M. (2009)**. Portable X-ray fluorescence spectrometry-capabilities for in situ analysis. Edited by P. J. Potts and M. West. RSC Publishing, Cambridge, UK, 2008, 291pp. **X-Ray Spectrometry**, **38**, 157.

Prettyman, **T.H.**, **Hagerty**, **J.J.**, **Elphic**, **R.C.**, **Feldman**, **W.C.**, **Lawrence**, **D.J.**, **McKinney**, **G.W.** and **Vaniman**, **D.T. (2006)**. Elemental composition of the lunar surface: Analysis of gamma ray

spectroscopy data from Lunar Prospector. **Journal of Geophysical Research: Planets**, **111**, n/a-n/a.

Radu, **T.** and **Diamond**, **D. (2009)**. Comparison of soil pollution concentrations determined using AAS and portable XRF techniques. **Journal of Hazardous Materials**, **171**, 1168–1171.

Righter, **K.**, **Collins**, **S.J.** and **Brandon**, **A.D. (2005)**. Mineralogy and petrology of the LaPaz Icefield lunar mare basaltic meteorites. **Meteoritics & Planetary Science**, **40**, 1703–1722.

Rochette, **P.** and **Gattacceca**, **J. (2012)**. Magnetic Classification of Meteorites and Application To the Sołtmany Fall. **Meteorites, 2**, 67–71.

Rochette, **P.**, **Gattacceca**, **J.**, **Bonal**, **L.**, **Bourot-Denise**, **M.**, **Chevrier**, **V.**, **Clerc**, **J.-P.**, **Consolmagno**, **G.**, **Folco**, **L.**, **Gounelle**, **M.**, **Kohout**, **T.**, **Pesonen**, **L.**, **Quirico**, **E.**, **Sagnotti**, **L.** and **Skripnik**, **A. (2008)**. Magnetic classification of stony meteorites: 2. Non-ordinary chondrites. **Meteoritics & Planetary Science**, **43**, 959–980.

Rochette, **P.**, **Gattacceca**, **J.**, **Bourot-Denise**, **M.**, **Consolmagno**, **G.**, **Folco**, **L.**, **Kohout**, **T.**, **Pesonen**, **L.** and **Sagnotti**, **L. (2009)**. Magnetic classification of stony meteorites: 3. Achondrites. **Meteoritics & Planetary Science Archives**, **44**, 405–427.

Rochette, **P.**, **Gattacceca**, **J.**, **Ivanov**, **A. V.**, **Nazarov**, **M.A.** and **Bezaeva**, **N.S. (2010)**. Magnetic properties of lunar materials: Meteorites, Luna and Apollo returned samples. **Earth and Planetary Science Letters**, **292**, 383–391.

Rochette, **P.**, **Gattacceca**, **J.**, **Menvielle**, **M.**, **Eisenlohr**, **P.** and **Chevrier**, **V. (2004)**. Interest and design of magnetic properties measurements on planetary and asteroidal landers. **Planetary and Space Science, 52,** 987–995.

Rochette, **P.**, **Sagnotti**, **L.**, **Bourot-Denise**, **M.**, **Consolmagno**, **G.J.**, **Folco**, **L.**, **Gattacceca**, **J.**, **Osete**, **M.L.** and **Pesonen**, **L. (2003)**. Magnetic classification of stony meteorites: 1. Ordinary chondrites. **Meteoritics & Planetary Science**, **38**, 251–268.

Rubin, **A.E.**, **Warren**, **P.H.**, **Greenwood**, **J.P.**, **Verish**, **R.S.**, **Leshin**, **L.A.**, **Hervig**, **R.L.**, **Clayton**, **R.N.** and **Mayeda**, **T.K. (2000)**. Los Angeles: the most differentiated basaltic martian meteorite. **Geology**, **28**, 1011–1014.

Shirai, **N.**, **Humayun**, **M.** and **Irving**, **A.J. (2009)**. The bulk composition of coarse-grained meteorites from laser ablation analysis of their fusion crusts. **40th Lunar and Planetary Science Conference,** Abstract 2170.

Takeda, **H.**, **Yamaguchi**, **A.**, **Bogard**, **D.D.**, **Karouji**, **Y.**, **Ebihara**, **M.**, **Ohtake**, **M.**, **Saiki**, **K.** and **Arai**, **T. (2006)**. Magnesian anorthosites and a deep crustal rock from the farside crust of the moon. **Earth and Planetary Science Letters, 247,** 171-184.

Tamponi, **M.**, **Bertoli**, **F.**, **Innocenti**, **F.** and **Leoni**, **L. (2003)**. X-ray fluorescence analysis of major elements in silicate rocks using fused glass discs. **Atti della Società Toscana di Scienze Naturali, Memorie Serie A**, **107**, 73–80.

Taylor, **G.J. (2009)**. Ancient Lunar Crust: Origin, Composition, and Implications. **Elements**, **5**, 17-23.

Tompkins, **S.** and **Pieters**, **C.M. (1999)**. Mineralogy of the lunar crust: Results from Clementine. **Meteoritics & Planetary Science**, **34**, 25–41.

Treiman, **A.H.**, **Gleason**, **J.D.** and **Bogard**, **D.D. (2000)**. The SNC meteorites are from Mars. **Planetary and Space Science**, **48**, 1213–1230.

Vanhoof, **C.**, **Holschbach-Bussian**, **K.A.**, **Bussian**, **B.M.**, **Cleven**, **R.** and **Furtmann**, **K. (2013)**. Applicability of portable XRF systems for screening waste loads on hazardous substances as incoming inspection at waste handling plants. **X-Ray Spectrometry**, **42**, 224–231.

Vázquez, **C.**, **Palacios**, **O.**, **Lué-Merú**, **M.**, **Custo**, **G.**, **Ortiz**, **M.** and **Murillo**, **M. (2012)**. Provenance study of obsidian samples by using portable and conventional X ray fluorescence spectrometers. Performance comparison of both instrumentations. **Journal of Radioanalytical and Nuclear Chemistry**, **292**, 367–373.

Wänke, **H.**, **Baddenhausen**, **H.**, **Dreibus**, **G.**, **Jagoutz**, **E.**, **Kruse**, **H.**, **Palme**, **H.**, **Spettel**, **B.** and **Teschke**, **F. (1973)**. Multielement analyses of Apollo 15, 16, and 17 samples and the bulk composition of the moon. **Proceedings of the Lunar Science Conference, 4**, 1461.

Warren, **H.P.**, **Kallemeyn**, **W.G.**, **Arai**, **T.** and **Kaneda**, **K. (1996)**. Compositional-petrologic investigation of eucrites and the QUE94201 Shergottite. **Antarctic Meteorites XXI. 21st Symposium on Antarctic Meteorites, NIPR, Tokyo, June 5-7**, **21**, 195–197.

Warren, **P.H. (2005)**. “New” lunar meteorites: Implications for composition of the global lunar surface, lunar crust, and the bulk Moon. **Meteoritics & Planetary Science Archives**, **40**, 477–506.

Warren, **P.H..**, **Ulff-Møller**, **F..** and **Kallemeyn**, **G.W.. (2005)**. “New” lunar meteorites: Impact melt and regolith breccias and large-scale heterogeneities of the upper lunar crust. **Meteoritics &**

Planetary Science, **40**, 989–1014.

Warren, **P.H.** and **Kallemeyn**, **G.W. (1993)**. Geochemical investigation of two lunar mare meteorites: Yamato-793169 and Asuka-881757. **Proceedings of the NIPR Symposium, No. 6**, 35–37.

Warren, **P.H.** and **Kallemeyn**, **G.W. (1991)**. The MacAlpine Hills lunar meteorite and implications of the lunar meteorites collectively for the composition and origin of the Moon. **Geochimica et Cosmochimica Acta**, **55**, 3123–3138.

Wiechert, **U.**, **Halliday**, **A.N.**, **Lee**, **D.-C.** and **Rumble**, **D. (2001)**. Oxygen Isotopes and the Origin of Tungsten Isotope Variations in Martian Meteorites. **64th Annual Meteoritical Society Meeting,** Abstract 5349.

Wu, **C.-M.**, **Tsai**, **H.-T.**, **Yang**, **K.-H.** and **Wen**, **J.-C. (2012)**. How Reliable is X-Ray Fluorescence (XRF) Measurement for Different Metals in Soil Contamination? **Environmental Forensics**, **13**, 110–121.

Yamaguchi, **A.**, **Karouji**, **Y.**, **Takeda**, **H.**, **Nyquist**, **L.**, **Bogard**, **D.**, **Ebihara**, **M.**, **Shih**, **C.-Y.**, **Reese**, **Y.**, **Garrison**, **D.**, **Park**, **J.** and **McKay**, **G. (2010)**. The variety of lithologies in the Yamato-86032 lunar meteorite: Implications for formation processes of the lunar crust. **Geochimica et Cosmochimica Acta**, **74**, 4507–4530.

Yamaguchi, **A.**, **Takeda**, **H.**, **Bogard**, **D.D.** and **Garrison**, **D. (1994)**. Textural variations and impact history of the Millbillillie eucrite. **Meteoritics**, **29**, 237–245.

Yanai, **K. (1994)**. Angrite Asuka-881371: Preliminary examination of a unique meteorite in the Japanese collection of Antarctic meteorites. **18th Symposium on Antarctic Meteorites. Proceedings of the NIPR Symposium**, **7**.

Yanai, **K.** and **Kojima**, **H. (1991)**. Meteorites recovered from antarctica. **Proceedings of the NIPR Symposium on Antarctic Meteorites**, **4**, 70–90.

Yanai, **K.** and **Kojima**, **H. (1984)**. Yamato-791197: A lunar meteorite in the Japanese collection of Antarctic meteorites. **Memoirs of National Institute of Polar Research. Special issue**, **35**, 18–34.

Young, **K.E.**, **Evans**, **C.A.**, **Hodges**, **K. V.**, **Bleacher**, **J.E.** and **Graff**, **T.G. (2016)**. A review of the handheld X-ray fluorescence spectrometer as a tool for field geologic investigations on Earth and in planetary surface exploration. **Applied Geochemistry**, **72**, 77–87.

Zeigler, **R.A.**, **Korotev**, **R.L.**, **Jolliff**, **B.L.** and **Haskin**, **L.A. (2005)**. Petrography and geochemistry of the LaPaz Icefield basaltic lunar meteorite and source crater pairing with Northwest Africa 032. **Meteoritics & Planetary Science**, **40**, 1073–1101.

Zipfel, **J. (2000)**. Sayh Al Uhaymir 005/008 and Its Relationship to Dar al Gani 476/489. **Meteoritics & Planetary Science, 35,** A178.

Zipfel, **J.**, **Scherer**, **P.**, **Spettel**, **B.**, **Dreibus**, **G.** and **Schultz**, **L. (2000)**. Petrology and chemistry of the new shergottite Dar al Gani 476. **Meteoritics & Planetary Science**, **35**, 95–106.

Zurfluh, **F.J.**, **Hofmann**, **B.A.**, **Gnos**, **E.** and **Eggenberger**, **U. (2011)**. Evaluation of the utility of handheld XRF in meteoritics. **X-Ray Spectrometry**, **40**, 449–463.

Figure and table captions

Figure 1. Picture showing the HH-EDXRF mobile test stand during the positioning of an eucrite. a) View from the front. b) View from the top.

Figure 2. Stereomicroscopic images showing the surfaces of four meteorites analyzed by HH-EDXRF. a) DaG 669 (howardite); b) NWA 3141 (eucrite); c) DEW 12007 (lunar, regolithic breccia); d) DaG 1062 (polymict eucrite). Textural and grain size variability are apparent. The circles provide a scale of the 8 mm x-ray beam diameter adopted in this study relative to the grain-size of the studied meteorites. Due to the relatively small sample size of NWA 3141, the 5 measured spots partially overlap with one another. Representative bulk composition have been obtained by multiple spots on each surface.

Figure 3. HH-EDXRF raw measurements plotted versus WD-XRF data of terrestrial igneous rock slabs. The dashed line represents the best-fit line. The solid line is the line of equation y=x.

Figure 4. HH-EDXRF corrected measurements plotted versus WD-XRF data of igneous rock slabs. The solid line is the line of equation y=x

Figure 5. Manganese vs Fe abundances (with 1 SD error bars) of HEDs (Millbillillie and Camel Donga), SNCs (Nakhla, SaU 008, Chassigny), and one angrite (D'Orbigny) determined by HH-EDXRF from different slabs of the same meteorite. Thick solid lines are trend lines for Vesta, Mars and the angrites parent body obtained from bulk compositional literature data (plotted as x for HEDs, * for SNCs and + for angrites) by different methods (ICP-MS, ICP-AES, INAA, ICP-OES, WD-XRF, EMPA on fused beads). Shaded areas represent the 68% confidence limit. Data are from (Mittlefehldt and Lindstrom 1990, Yanai 1994, Mittlefehldt *et al.* 2002, Jambon *et al.* 2005, Gellissen *et al.* 2007, Shirai *et al.* 2009, Keil 2012) for angrites; from (Dreibus *et al.* 1996, Warren *et al.* 1996, Lodders and Fegley 1998, Folco *et al.* 2000, Rubin *et al.* 2000, Zipfel *et al.* 2000, Barrat *et al.* 2002, Jambon *et al.* 2002, Anand *et al.* 2005, Barrat *et al.* 2006, Beck *et al.* 2006, Irving *et al.* 2011, Kuehner *et al.* 2011) for SNCs; from Mittlefehldt (2015) and references therein for HEDs.

Figure 6. Fe/Mn ratio (with 1 SD error bars) for angrites, lunar, SNC and HED meteorites, and the terrestrial igneous rocks used for calibration. Dashed lines denote mean literature values for each meteorite class. Gray shaded areas represent 1 SD. Data for HEDs, SNCs and angrites are reported in the caption of Figure 5. Data for lunar meteorites are from (Yanai and Kojima 1984, Lindstrom *et al.* 1991, Warren and Kallemeyn 1991, Yanai and Kojima 1991, Warren and Kallemeyn 1993, Bischoff *et al.* 1998, Fagan *et al.* 2002, Anand *et al.* 2003, Demidova *et al.* 2003, Fagan *et al.* 2003, Korotev *et al.* 2003, Righter *et al.* 2005, Warren *et al.* 2005, Zeigler *et al.* 2005, Anand *et al.* 2006, Joy *et al.* 2006, Haloda *et al.* 2006, Nyquist *et al.* 2006, Demidova *et al.* 2007, Greshake *et al.* 2008, Joy *et al.* 2008, Haloda *et al.* 2009, Korotev *et al.* 2009, Liu *et al.* 2009, Collareta *et al.* 2016, Mészáros *et al.* 2016). Data for terrestrial basalts are from IGBA database (Brändle and Nagy

1995).

Figure 7. a) Plot of Si vs Fe/Mn ratio for lunar meteorites and angrites. b) Ca/K values (log scale) vs. Fe/Mn ratio for Martian meteorites and HEDs. The compositional variability reflects variations in the modal abundances of ultramafic and basaltic minerals. Literature data, plotted for comparison, are from references reported in the caption of Figure 5.

Figure 8. Manganese vs. Fe abundance for the fusion crusts and the interior composition of selected HEDs (a) and SNC meteorites (b). Filled symbols represent the composition of the interior. Empty symbols denote the fusion crust. Asterisks indicate interior and fusion crusts, analysed by McCarthy et al. (1973), Mittlefehldt (1979), Genge and Grady (1999) and Gnos et al. (2002) through EMPA. Thick solid lines are linear fit functions. Shaded areas represent 68% confidence limit and dashed lines 95% confidence limit. Regression lines and confidence limits are calculated from literature data also plotted for comparison (small symbols). References are reported in the caption of Figure 5.

Figure 9. Fe/Mn ratio vs magnetic susceptibility (Logχ 10-9 m3/kg) for four angrites, three lunar meteorites, nine SNCs and ten HEDs. Fe/Mn values are from Table 4, Logχ values are from (Rochette *et al.* 2009, Rochette *et al.* 2010, Collareta *et al.* 2016). The boxes representing the Fe/Mn ratios and Logχ values of ordinary and enstatite chondrites (falls) and carbonaceous chondrite (finds) are also plotted for comparison. Errors bar are 1 SD. Dashed lines denote mean literature values for each meteorite class. Gray shaded areas represent 1 SD. Data for HEDs, SNCs, lunar and angrites are reported in the caption of Figures 5 and 6. Fe/Mn values for chondritic meteorites are from Nittler et al. 2004, while Logχ values are from (Rochette et al. 2003, 2008, 2009).

Table 1. HH-EDXRF operating condition used during measurements.

Table 2. List of the meteorites analysed in this work.

Table 3. Corrected HH-EDXRF data of the studied meteorites (% m/m). Each entry represents the mean of five or three measurements. See main text for explanation. Samples are listed in the same order of Table 2.

Supporting Information

Figure and table captions

Figure S1. Comparison between Mg concentrations determined by HH-EDXRF analyses of igneous rock slabs performed in this work and by Young et al. (2016). Both data sets are plotted versus reference values obtained by WD-XRF. The relatively high accuracy of our data, which plot close to the 1:1 line (solid line), are in obvious contrast with the more scattered data by Young et al. (2016).

Table S1. HH-EDXRF and WD-XRF analyses of terrestrial igneous rock slabs used for calibration. All elements in % m/m.

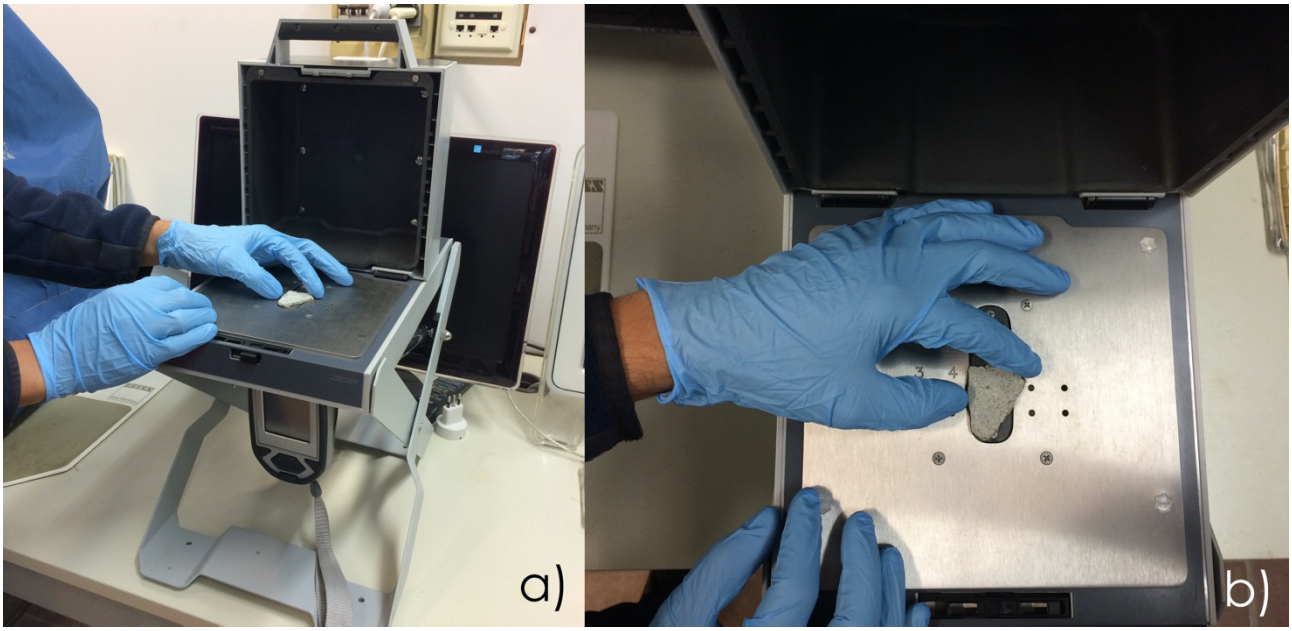

Figure 1

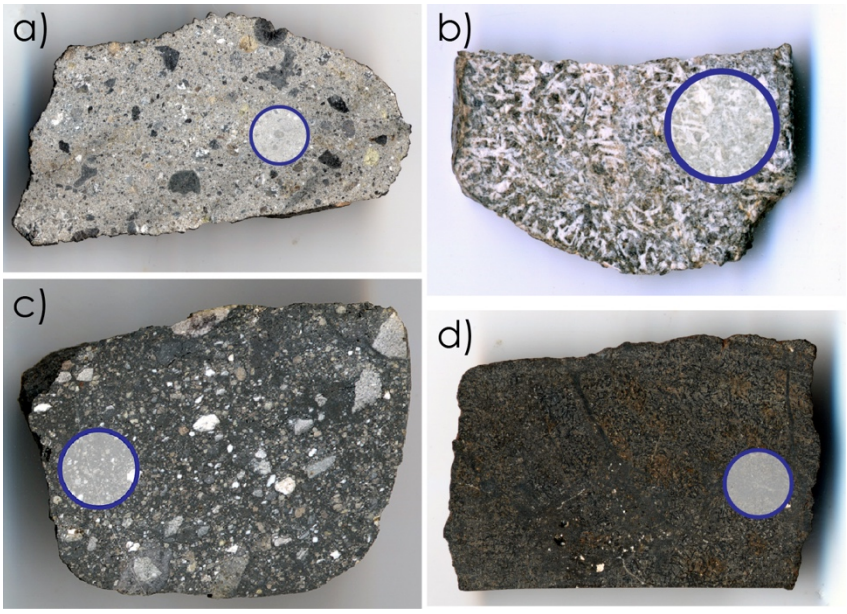

Figure2

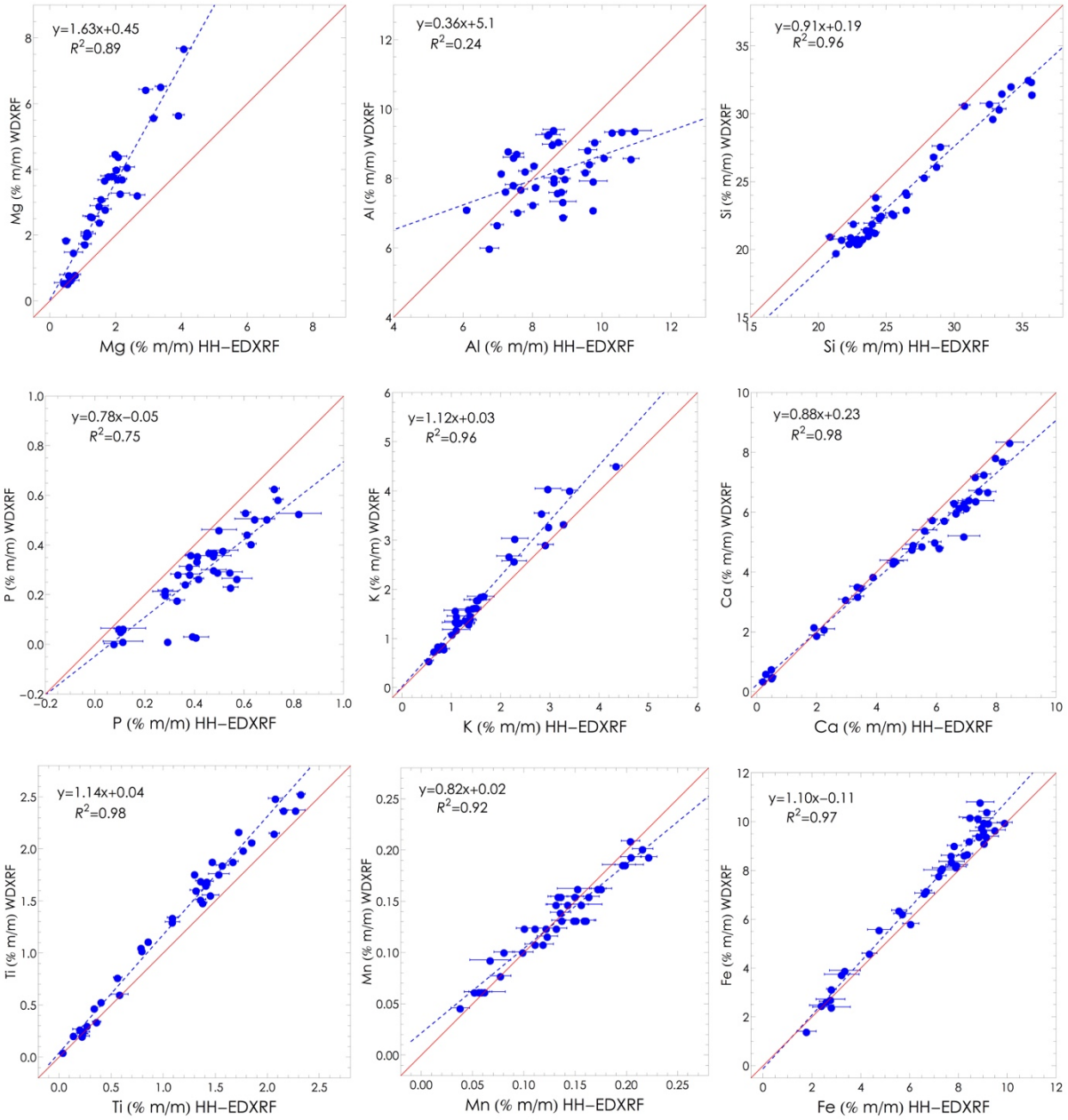
y=1.63x+0.45
R2=0.89
Mg (% m/m) WDXRF
Mg (% m/m) HH–EDXRF
y=0.36x+5.1
R2=0.24
Al (% m/m) WDXRF
Al (% m/m) HH–EDXRF
y=0.91x+0.19
R2=0.96
Si (% m/m) WDXRF
Si (% m/m) HH–EDXRF
y=0.78x–0.05
R2=0.75
P (% m/m) WDXRF
P (% m/m) HH–EDXRF
y=1.12x+0.03
R2=0.96
K (% m/m) WDXRF
K (% m/m) HH–EDXRF
y=0.88x+0.23
R2=0.98
Ca (% m/m) WDXRF
Ca (% m/m) HH–EDXRF
y=1.14x+0.04
R2=0.98
Ti (% m/m) WDXRF
Ti (% m/m) HH–EDXRF
y=0.82x+0.02
R2=0.92
Mn (% m/m) WDXRF
Mn (% m/m) HH–EDXRF
y=1.10x–0.11
R2=0.97
Fe (% m/m) WDXRF
Fe (% m/m) HH–EDXRF

Figure3

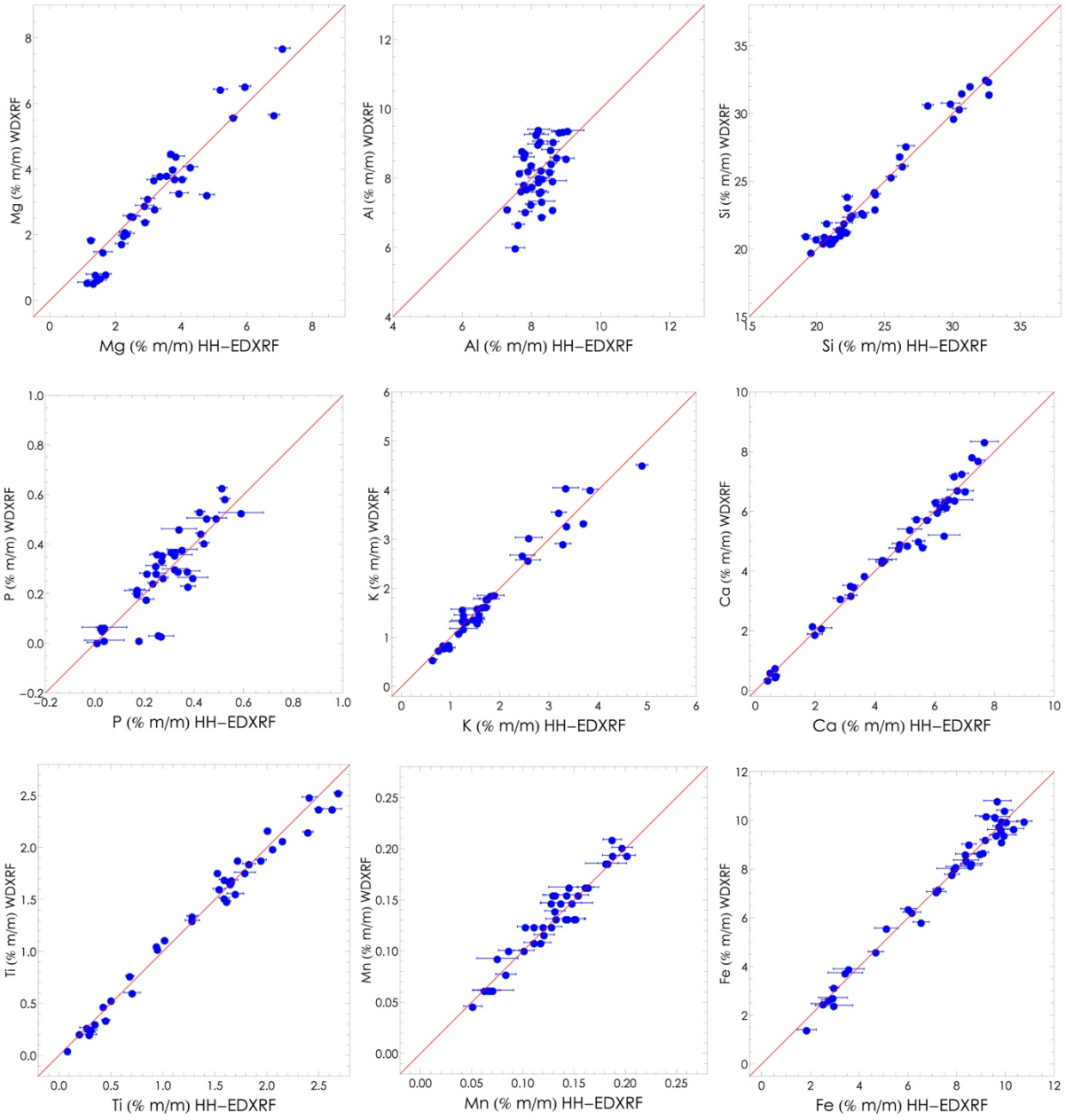
Mg (% m/m) WDXRF
Mg (% m/m) HH–EDXRF
Al (% m/m) WDXRF
Al (% m/m) HH–EDXRF
Si (% m/m) WDXRF
Si (% m/m) HH–EDXRF
P (% m/m) WDXRF
P (% m/m) HH–EDXRF
K (% m/m) WDXRF
K (% m/m) HH–EDXRF
Ca (% m/m) WDXRF
Ca (% m/m) HH–EDXRF
Ti (% m/m) WDXRF
Ti (% m/m) HH–EDXRF
Mn (% m/m) WDXRF
Mn (% m/m) HH–EDXRF
Fe (% m/m) WDXRF
Fe (% m/m) HH–EDXRF

Figure4

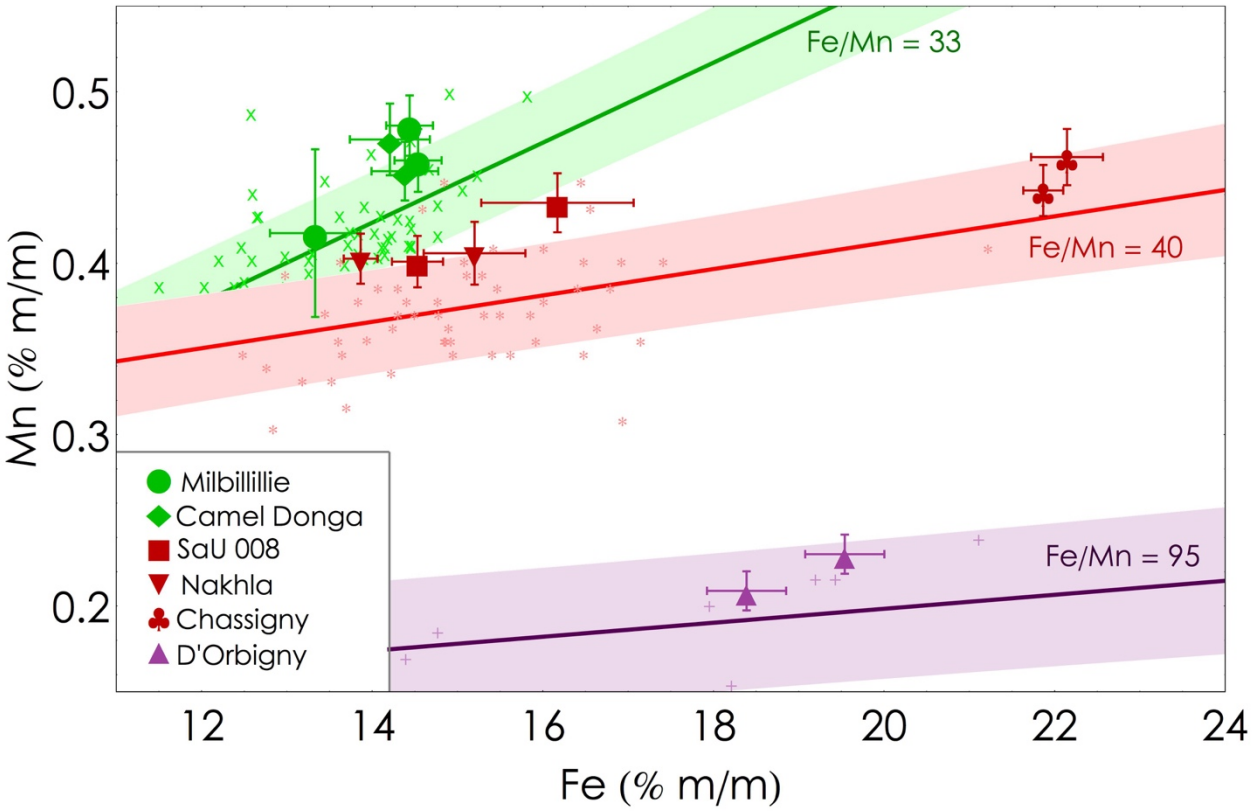
Fe/Mn = 33
Fe/Mn = 40
Fe/Mn = 95
Milbillillie
Camel Donga
SaU 008
Nakhla
Chassigny
D'Orbigny
Mn (% m/m)
Fe (% m/m)
0.2
0.3
0.4
0.5
12
14
16
18
20
22
24

Figure5

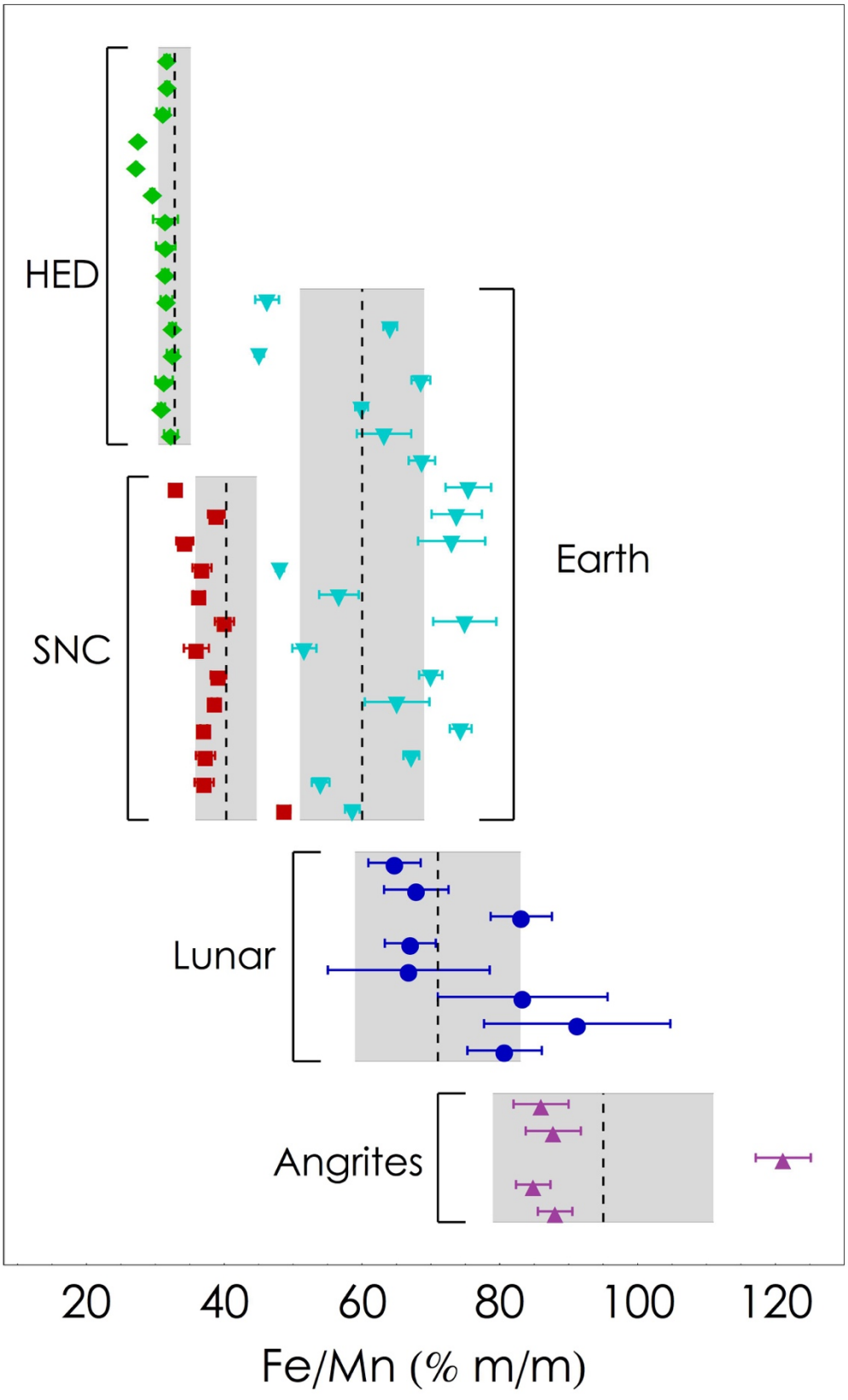

Figure6

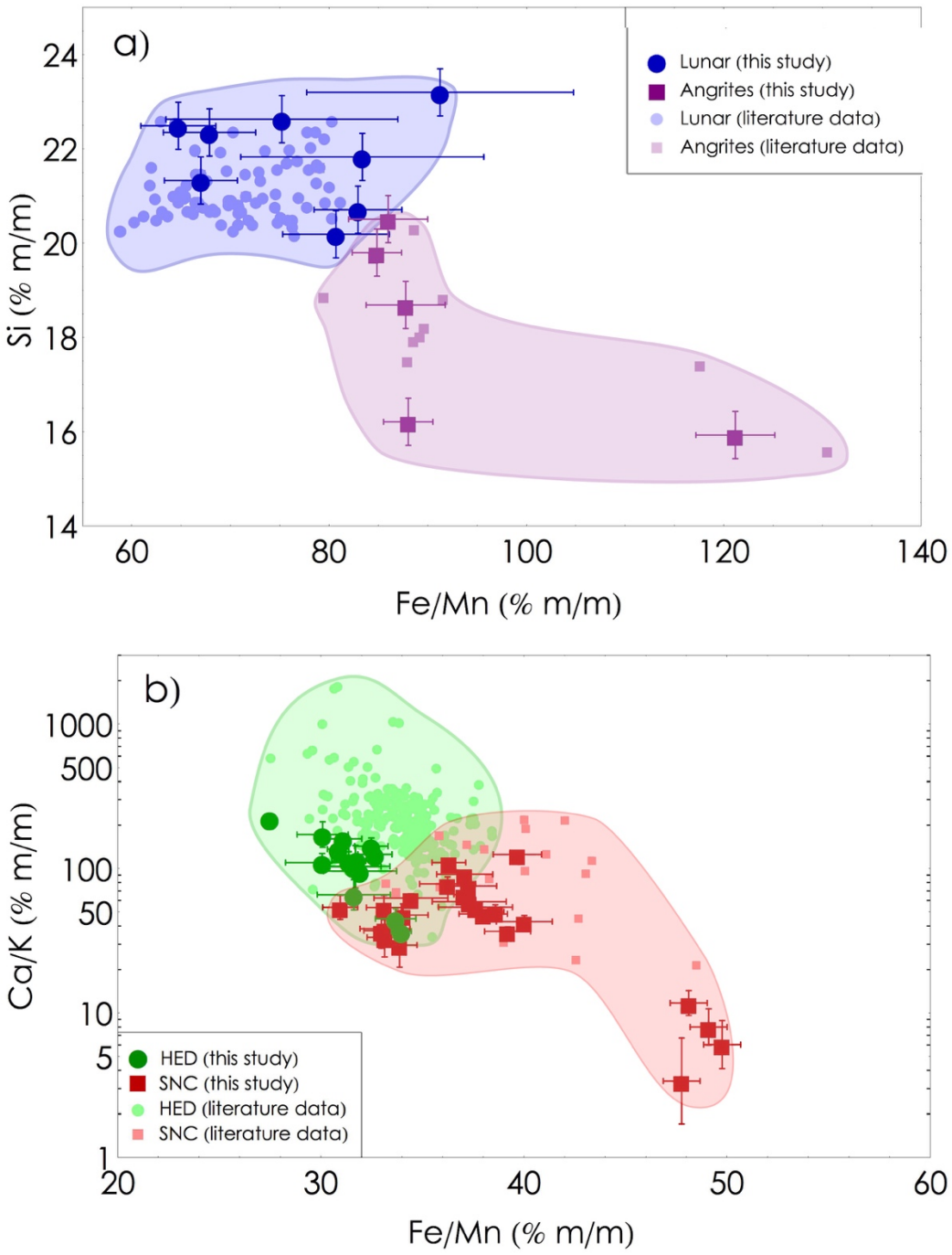

Figure7 con campi

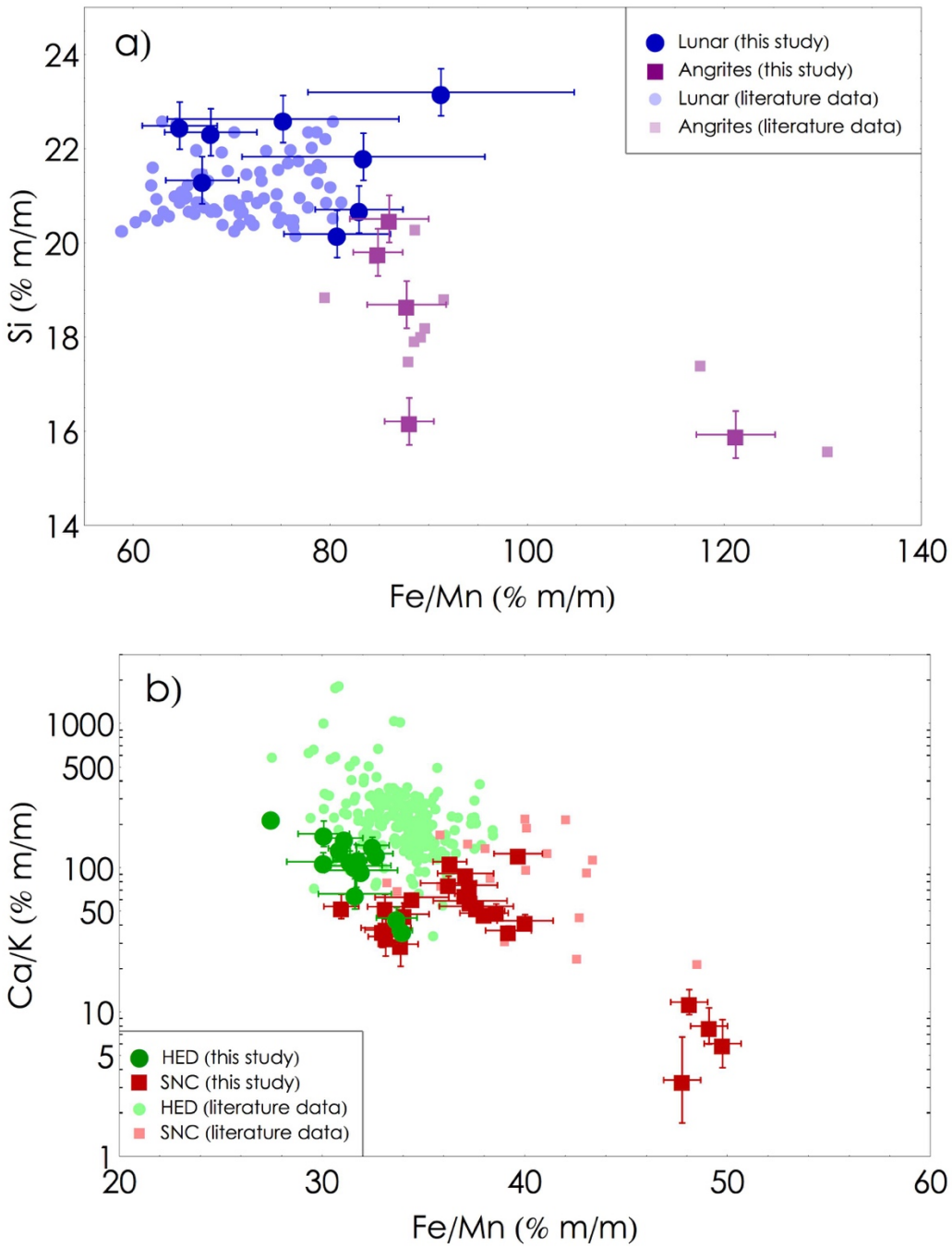

Figure7 no campi

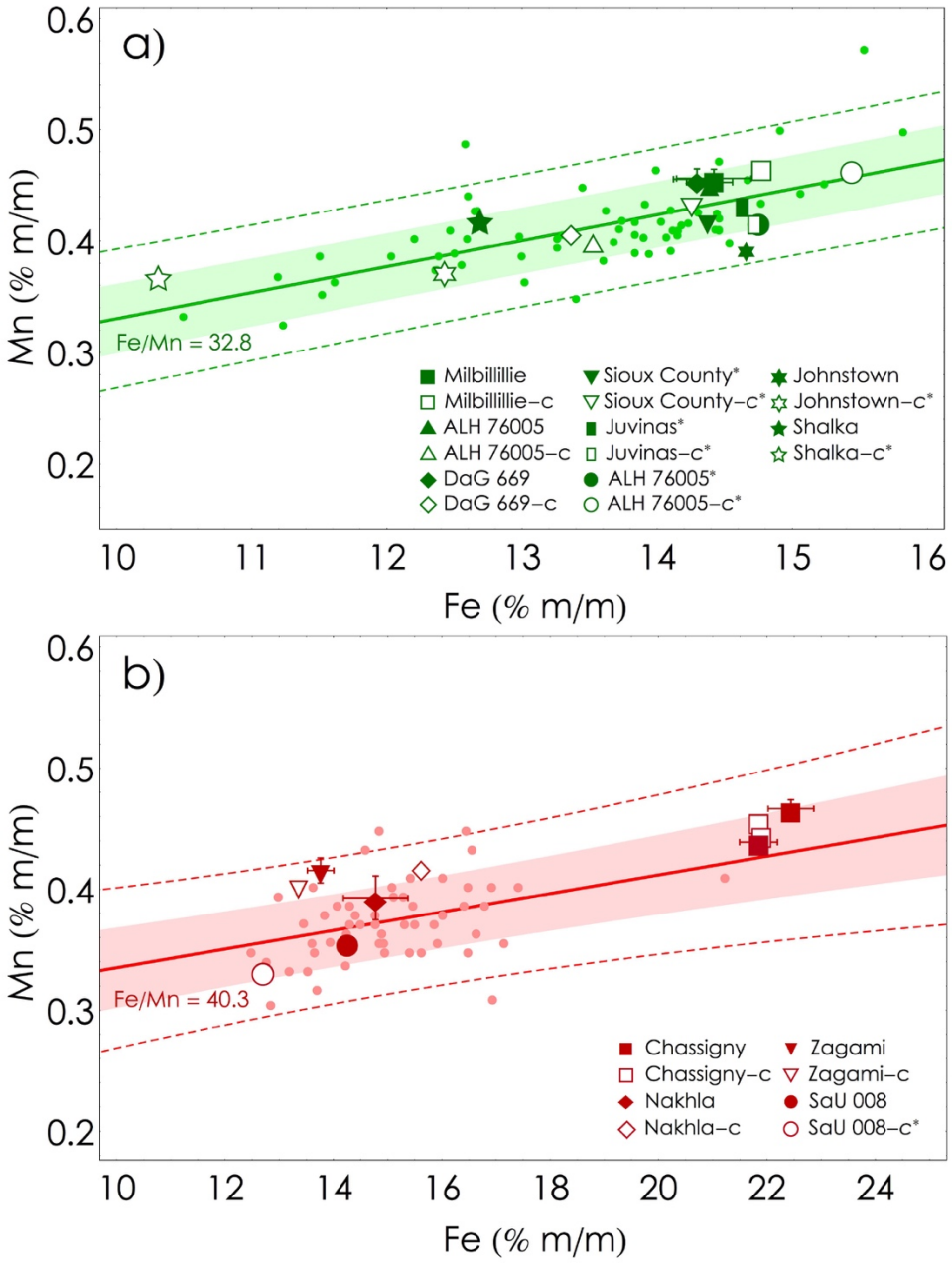
a)
Mn (% m/m)
Fe (% m/m)
Fe/Mn = 32.8
Milbillillie
Milbillillie–c
ALH 76005
ALH 76005–c
DaG 669
DaG 669–c
Sioux County*
Sioux County–c*
Juvinas*
Juvinas–c*
ALH 76005*
ALH 76005–c*
Johnstown
Johnstown–c*
Shalka
Shalka–c*
b)
Mn (% m/m)
Fe (% m/m)
Fe/Mn = 40.3
Chassigny
Chassigny–c
Nakhla
Nakhla–c
Zagami
Zagami–c
SaU 008
SaU 008–c*

Figure8

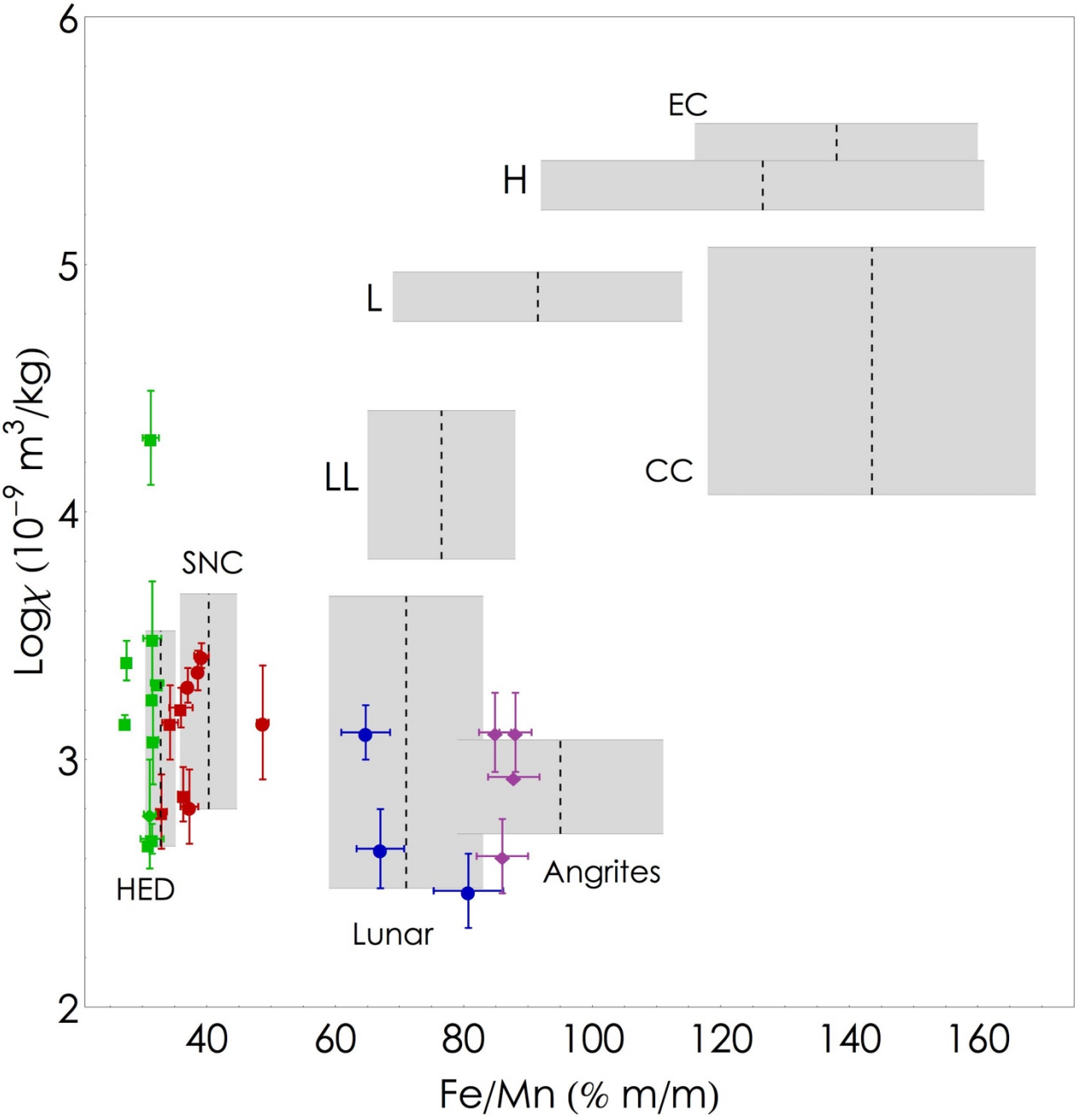
EC
H
L
LL
CC
SNC
HED
Lunar
Angrites
Logχ (10^{-9} m^3/kg)
Fe/Mn (% m/m)
6
5
4
3
2
40
60
80
100
120
140
160

Figure9